Title Page

TAK1: a potential therapeutic target for retinal neovascularization

Fan-Li Lin[1,2†], Jiang-Hui Wang[3†], Jinying Chen[2,4], Linxin Zhu[2,4], Yu-Fan Chuang[1,2], Leilei Tu[4], Chenkai Ma[5], Suraj Lama[2], Damien Ling[3], Raymond Ching-Bong Wong[3,6], Alex W. Hewitt[2,3], Ching-Li Tseng[7], Bang V. Bui[8], Peter van Wijngaarden[3,6], Gregory J. Dusting[3,6], Peng-Yuan Wang[1], Guei-Sheung Liu[2,6,9*]

[1]Shenzhen Key Laboratory of Biomimetic Materials and Cellular Immunomodulation, Shenzhen Institute of Advanced Technology, Chinese Academy of Sciences, Shenzhen, China

[2]Menzies Institute for Medical Research, University of Tasmania, Hobart, Australia

[3]Centre for Eye Research Australia, Royal Victorian Eye and Ear Hospital, East Melbourne, Australia

[4]Department of Ophthalmology, the First Affiliated Hospital of Jinan University, Guangzhou, China

[5]Molecular Diagnostics Solutions, CSIRO Health and Biosecurity, North Ryde, New South Wales, Australia

[6]Ophthalmology, Department of Surgery, University of Melbourne, East Melbourne, Victoria, Australia

[7]Graduate Institute of Biomedical Materials and Tissue Engineering, College of Biomedical Engineering, Taipei Medical University, Taipei, Taiwan

[8]Department of Optometry and Vision Sciences, University of Melbourne, Parkville, Victoria, Australia

[9]Aier Eye Institute, Changsha, Hunan, China

†FLL and JHW contributed equally to this work.

*Correspondence and requests for materials should be addressed to Dr Guei-Sheung Liu (rickliu0817@gmail.com). Menzies Institute for Medical Research, University of Tasmania. Address: 17 Liverpool Street, Hobart, TAS 7000, Australia. Tel: +61362264250.

Running title: Targeting TAK1 alleviates retinal neovascularization

Key words: Transforming growth factor-β-activated kinase 1, inflammation, angiogenesis, retinal neovascularization, oxygen-induced retinopathy

ABSTRACT

Retinal neovascularization, or pathological angiogenesis in the retina, is a leading cause of blindness in developed countries. Pathological angiogenesis occurs through the complex activation of pro-inflammatory and pro-angiogenic pathways. Transforming growth factor-β-activated kinase 1 (TAK1) is a mitogen-activated protein kinase kinase kinase (MAPKKK) activated by TGF-β1 and other pro-inflammatory cytokines such as tumor necrosis factor α (TNFα) and interleukin-1 (IL-1). TAK1 is a key mediator of inflammation, innate immune responses, apoptosis and tissue homeostasis and plays an important role in physiological angiogenesis. Its role in pathological angiogenesis, particularly in retinal neovascularization, remains unclear. We investigated the regulatory role of TAK1 in pathological angiogenesis in the retina. Transcriptome analysis of human retina featuring retinal neovascularization revealed enrichment of known TAK1-mediated signaling pathways. Genetic or pharmacological inhibition of TAK1 activation in human endothelial cells induced by TNFα or IL-1 stimulation led to inhibition of phosphorylation of major kinases, including nuclear factor kappa B (NFκB) and mitogen-activated protein kinase (MAPK) signaling pathways. Suppression of this signaling, in turn, decreased expression of downstream genes associated with inflammation and angiogenesis, suggesting that TAK1 is required for these pathological processes. Transcriptome analysis of endothelial cells revealed that TAK1 knockout prevented inflammatory and immune responses induced by TNFα stimulation, mainly via cytokine and chemokine activity. Selective inhibition of TAK1 by 5Z-7-oxozeaenol *in vitro* ameliorated pro-angiogenic activity, including endothelial cell proliferation, migration and tube formation. Moreover, 5Z-7-oxozeaenol attenuated aberrant retinal angiogenesis in rats following oxygen-induced retinopathy. Our finding shows that TAK1 plays a key role in pathological angiogenesis in the retina. Selective inhibition of TAK1 prevents pathological angiogenesis, suggesting that TAK1 could be a potential therapeutic target for retinal neovascularization.

58 **GRAPHICAL ABSTRACT**

59

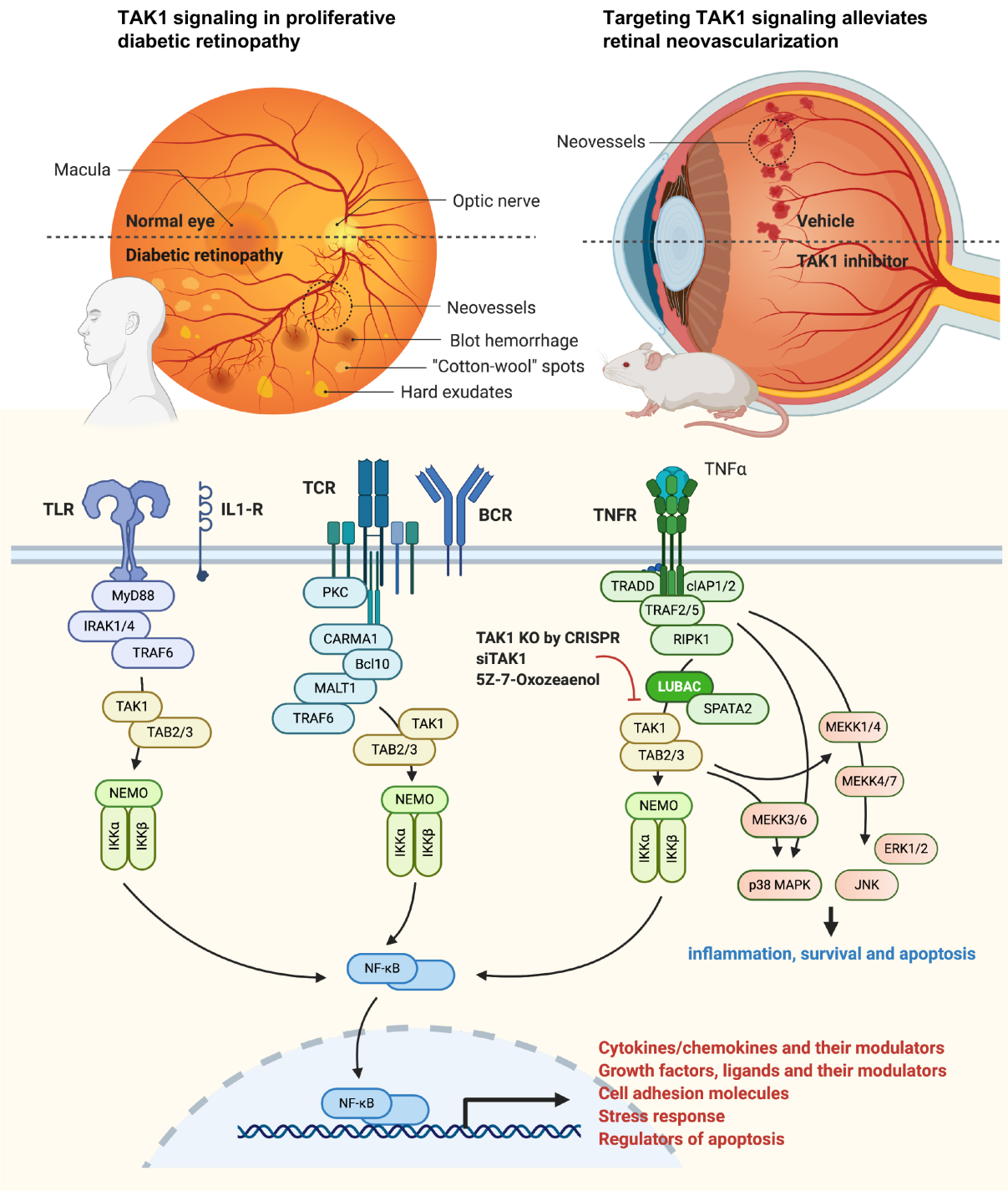

60

61 **INTRODUCTION**

62 Retinal neovascularization is a severe complication of several ocular diseases, often resulting in
63 permanent damage to the neurosensory retina and irreversible vision loss (*1*). Retinal
64 neovascularization shares similar characteristics to pathological angiogenesis elsewhere in the body,
65 exhibiting features including endothelial proliferation and migration, elevated vascular permeability
66 and inflammation; all processes in which vascular endothelial growth factor (VEGF) plays a crucial
67 role (*2*). Recently, the advent of ocular anti-VEGF therapies has been a significant advance in
68 mitigating the risk of vison loss associated with retinal neovascularization. Despite this success, there
69 is increasing evidence that some patients do not respond well to anti-VEGF treatments (*3*). Therefore,
70 it is necessary to seek other therapeutic targets.

71 The common pathways shared between inflammation and angiogenesis play critical roles in
72 retinal neovascularization (*4*). Several studies have reported increased expression of various pro-
73 inflammatory cytokines, chemokines, pro-angiogenic factors and adhesion molecules in patients with
74 retinal neovascularization, such as tumor necrosis factor α (TNFα), interleukin-1 (IL-1), chemokine
75 (C-X-C motif) ligand 8 (CXCL8; known as IL-8), vascular endothelial growth factor (VEGF), as well
76 as intercellular adhesion molecule 1 (ICAM-1) (*5-9*). TNFα was found to suppress the expression of
77 tight junction proteins and is required for VEGF-mediated hyperpermeability in endothelial cells and
78 the breakdown of the blood-retinal barrier in patients with diabetic retinopathy (DR) (*10, 11*).
79 Interleukins are also primary mediators of inflammation that can promote angiogenesis via induction
80 of proangiogenic factors such as VEGF (*4*). Moreover, TNFα and IL-1 stimulates expression of ICAM-
81 1, CXCL8 and VEGF in endothelial cells and microglia cells, both of which promote progression of
82 retinal neovascularization (*12, 13*). A key role for inflammatory mediators is highlighted by their
83 growing use as prognostic markers of the severity of proliferative diabetic retinopathy (PDR) (*4*).

84 Transforming growth factor-β-activated kinase 1 (TAK1), a member of the mitogen-activated
85 protein kinase (MAPK) family, is a critical serine/threonine kinase in several cellular signaling
86 pathways. Such pathways can be activated by diverse pro-inflammatory stimuli including TNFα, IL-
87 1, transforming growth factor beta (TGF-β), or toll-like receptor (TLR) ligands. The engagement of
88 TAK1 in turn activates downstream signaling pathways, including nuclear factor kappa B (NFκB) and
89 MAPK p38, extracellular signal-regulated kinase (ERK), and c-Jun kinase (JNK) signaling,
90 modulating inflammatory responses and cell survival (*14-16*). TAK1 inhibition has been shown to
91 reduce TNFα and CXCL8 secretion in leukocytes (*17*) and to suppress prostaglandin-endoperoxide
92 synthase 2 (PTGS2; known as cyclooxygenase-2, COX-2), ICAM-1, and VEGF expression in cancer
93 cells through NFκB signaling pathway (*18*). Expression of TAK1 provides protection for endothelial
94 cells against TNFα-induced apoptosis under inflammatory conditions (*19*). Indeed, TAK1 deletion

95 causes embryonic lethality as the capacity to prevent TNFα-induced endothelial cell death and vessel
96 regression is lost. Moreover, TAK1 is also important for supporting TNFα-independent vascular
97 formation and endothelial migration. These broad roles for TAK1 suggests that endothelial TAK1
98 inhibition may be a useful alternate anti-angiogenesis target in retinal disease (*19, 20*).
99 We hypothesized that TAK1 plays a crucial role in pathological angiogenesis and TAK1 inhibition
100 can suppress retinal neovascularization. Our findings indicate that TAK1 is an important regulator of
101 inflammatory and angiogenesis-related pathways that contribute to retinal neovascularization.
102 Pharmacological inhibition of TAK1 alleviated aberrant retinal angiogenesis by modulating pro-
103 inflammatory and pro-angiogenic signaling in a rat model of ischemia-induced retinopathy.
104
105
106 **RESULTS**
107 **TAK1 is expressed in human retina and is positively associated with retinal neovascularization**
108 To understand TAK1 expression profiles in the human retina, we first analyzed published of single
109 nuclei RNAseq (snRNAseq, GSE135133) data to examine TAK1 expression in different retinal cells.
110 Analysis of 121,799 individual cells from human retina revealed that both *TAK1* (*MAP3K7*) and its
111 binding protein, *TAB1-3,* are expressed moderately in most neural and non-neural retinalcells (**Fig. 1A**
112 **and S1**). Notably, among the retinal cells examined, TAK1 is highly enriched in endothelial cells.
113 Immunostaining suggests that TAK1 is expressed in various layers of the human retina in both neural
114 and non-neural cells, such as mural cells including smooth muscle cells (**Fig. 1B**) in larger vessels
115 (diameter of artery or vein ranging from 0.6 - 16 mm) (*21*). We also found that co-localization of
116 TAK1 and endothelial cell marker CD31 was more likely to be found in the microvasculature,
117 including arterioles or venules (20 - 25 μm) and capillaries (9 μm).
118 To identify the key molecular signaling or biological pathways relevant to the angiogenic process
119 in patients with retinal neovascularization, a transcriptome dataset from humans with proliferative
120 diabetic retinopathy (PDR) was interrogated by taking advantage of Gene Set Enrichment Analysis
121 (GSEA), a knowledge-based approach for interpreting genome-wide expression profiles (*22*).
122 Compared with controls those with retinal neovascularization showed enrichment of known TAK1
123 upstream signaling pathways, including IL1, TNF, TGF-β, TLR, T-cell receptor (TCR) and B-cell
124 receptor (BCR) (**Fig. 1C, S2 and S3A**). Pathways related directly to TAK1 were enriched, such as
125 "TAK1 activation of NFκB by phosphorylation and activation of inhibitor of κB (IκB) kinase (IKK)
126 complex", and "activated TAK1 mediated p38 MAPK activation" (**Fig. 1C and S3B**). There was
127 general upregulation of genes associated with the TAK1 activates NFκB by phosphorylation pathway

128 and activation of IKK complex pathway in patients with retinal neovascularization compared with
129 controls (**Fig. 1D and 1E**). There was negative enrichment of genes associated with several biological
130 pathways in relation to visual phototransduction and neuronal systems (**Fig 1C**).
131
132 **TAK1 is required for activation of NFκB signaling in the endothelial response to inflammatory**
133 **insults**
134 Previous studies have indicated that TAK1 is activated in response to various pro-inflammatory stimuli
135 such as TNFα, IL-1β, TGF-β, or TLR ligand: these stimulate mediators downstream of TAK1, such as
136 inflammatory cytokines - CXCL8 and PTGS2 or antiapoptotic proteins-inhibitor of apoptosis (IAPs)
137 family, through both NFκB and MAPK pathways (*16, 23*). To evaluate what signaling regulates TAK1
138 in the endothelial response to inflammation, we generated TAK1-knockout (KO) human telomerase-
139 immortalized microvascular endothelial (TIME) cells (TAK1-KO) using CRISPR/Cas9 (**Fig. 2A-2D**).
140 To explore the role of TAK1 in endothelial cells, we generated a transcriptome through RNA
141 sequencing (RNA-seq) of wild type TIME cells (WT) and TAK1-KO TIME cells (TAK1-KO). We
142 found that 2178 genes were differentially expressed [false discovery rate (FDR), <0.05] following
143 TAK1-KO (**Fig. S4A and S4B**). GSEA results suggested that TAK1 knockout negatively affected
144 pathways related to immune responses and inflammation, such as interferon signaling (**Fig. S4C**).
145 Since TNFα is strongly correlated with progression of retinal neovascularization and it is a major
146 activator of TAK1 signaling (*10*), we used TNFα as the stimulus for *in vitro* studies. Treatment with
147 TNFα significantly increased TAK1 phosphorylation in wild-type cells, an effect not observed in
148 TAK1-KO cells (**Fig. 2E and 2F**). IκB degradation and NFκB p65 phosphorylation are key events in
149 NFκB signaling (*24*). TNFα significantly induced NFκB p65 phosphorylation and IκB degradation in
150 wild-type cells, while no such changes occurred in TAK1-KO cells (**Fig. 2E and 2G**). Likewise,
151 phosphorylation of JNK, p38, and ERK in MAPK signaling was not increased in TNFα-treated TAK1-
152 KO cells compared to TNFα-treated wild-type cells (**Fig. 2E and 2H**). Collectively, these data indicate
153 that TAK1 is required for phosphorylation of the key mediators of NFκB and MAPK signaling in
154 human microvascular endothelial cells.
155 To explore the effects of TAK1-KO in TIME cells upon TNFα stimulation, we generated two
156 more transcriptomes by RNA sequencing TNFα-treated wild type (WT) TIME cells and TNFα-treated
157 TAK1-KO TIME cells. We found that 462 and 263 genes were differentially expressed (FDR<0.05
158 and Log2FoldChange >1 or <-1) in wild type cells upon TNFα treatment (WT vs WT TNFα; hereafter
159 referred to as the WT TNFα set) and TAK1-KO cells upon TNFα treatment (TAK1-KO vs TAK1-KO
160 TNFα; hereafter referred to as the TAK1-KO TNFα set), respectively. The principal components
161 analysis of our dataset revealed a complete separation of four groups of samples (n=4 in each group,

162 **Fig. S5A-5C**). In keeping with the notion that TNFα induces TAK1-related signaling, we next sought
163 genes that are differentially expressed between WT TNFα and TAK1-KO TNFα sets. We observed
164 that 246 and 110 genes were exclusively up-regulated and down-regulated in WT TNFα set and not
165 the TAK1-KO TNFα set, suggesting these dysregulated genes were not induced by TNFα due to
166 TAK1-KO (**Fig. 3A and 3B**). Gene Ontology (GO) enrichment analysis of the 246 exclusively up-
167 regulated genes in the WT TNFα set suggested that TNFα stimulated inflammatory and immune
168 responses (**Fig. S6A**), mainly via cytokine and chemokine activity (**Fig. S6B**) while such TNF
169 responses did not occur in TAK1-KO TIME cells.

170 To further explore the biological significance of our differential expression findings, we
171 undertook GSEA of WT TNFα and TAK1-KO TNFα sets. This demonstrated a marked inflammatory
172 response via the NFκB pathway in cells stimulated by TNFα; however, activation of the NFκB
173 pathway was significantly reduced in TAK1-KO cells (**Fig. 3C**), confirming TNFα-induced
174 inflammation is mainly dependent on NFκB activation through TAK1. In keeping with the notion that
175 NFκB is the main regulator of immune responses and inflammation, and is also involved in cellular
176 apoptosis and cell cycle regulation (*25*), we selected five major biological functions regulated by NFκB
177 from a NFκB target gene database (*26*) to investigate the differential expression of included genes in
178 each function category between WT TNFα set and TAK1-KO TNFα set (**Table 1**). These functions
179 include cytokines/chemokines and their modulators, cell adhesion molecules, stress response, growth
180 factors, ligands and their modulators, and regulators of apoptosis. The results showed that most genes
181 in each functional category were significantly expressed in the WT TNFα set but were remarkably
182 suppressed in the TAK1-KO TNFα set (**Fig. S7-S11**), indicating all these functions induced by TNFα
183 were negatively affected in cells due to TAK1-KO. Expression of the most significant genes (those
184 also shown to be involved in retinal neovascularization) from each functional category in each group
185 was also validated using qRT-PCR (**Fig. 3D**). Upon TNFα stimulation, the expression level of *ICAM-*
186 *1*, *PTGS2*, *CXCL8* and *VEGF-A* were substantially elevated in wild-type cells, while no TNFα induced
187 change was observed in TAK-1 KO cells (**Fig. 3D**). Similar results were found in IL1β-treated wild-
188 type cells but not in IL1β-treated, TAK1-KO cells (**Fig. S12**). Likewise, TAK1 knockdown using
189 TAK1 siRNA (siTAK1) resulted in a significant anti-inflammatory effect in both TIMEs (**Fig. S13A,**
190 **S13B and S13E**) and human retinal microvascular endothelial cells (HRMECs) (**Fig. S13C and S13F**).
191 Interestingly, TAK1 knockdown only decreased expression of *ICAM-1* in Müller cells upon TNFα
192 treatment, but the siRNA increased expression of *PTGS2* and *CXCL8* and had no effects on *VEGF-A*
193 (**Fig. S13D and S13G**). These data further confirmed that TAK1 regulates a range of cellular functions
194 depending on the retinal cell type.

195

196 **Pharmacological inhibition of TAK1 suppresses inflammation-mediated angiogenic signaling**
197 **and pro-angiogenic activities *in vitro***

198 5Z-7-oxozeaenol, a resorcylic acid lactone derived from a fungus, is a selective inhibitor of TAK1
199 (*27*). We tested the effects of 5Z-7-oxozeaenol in human microvascular endothelial cells stimulated
200 with TNFα. Similar to TAK1-KO, 5Z-7-oxozeaenol significantly suppressed TNFα induced
201 phosphorylation of NFκB p65 (**Fig. 4A and 4B**), JNK, p38, and ERK (**Fig. S14**), indicating that 5Z-
202 7-oxozeaenol inhibits NFκB and MAPKs signaling in a dose-dependent manner. Consistent with the
203 anti-inflammatory effects observed in TAK1 knockout endothelial cells, 5Z-7-oxozeaenol inhibited
204 TNFα-induced expression of pro-inflammatory or pro-angiogenic genes, *PTGS2*, *CXCL8* and *ICAM-*
205 *1* as well as *VEGF-A* expression (**Fig. 4C**). This inhibitory effect of 5Z-7-oxozeaenol was also found
206 in HRMECs stimulated with TNFα (**Fig. 4D**). We also observed similar inhibitory effects of 5Z-7-
207 oxozeaenol stimulated with IL1β in HRMECs (**Fig. S15**).

208 In addition to examining the pro-angiogenic signals mediated by TAK1 in response to
209 inflammatory insult, we further investigated the involvement of TAK1 in various endothelial functions
210 related to angiogenesis through *ex vivo* and *in vitro* assays. We first used an *ex vivo* aortic ring
211 sprouting assay to test the anti-angiogenic effects of pharmacological TAK1 inhibition by 5Z-7-
212 oxozeaenol. We found that vascular sprouting was significantly suppressed 3 days (45.9%) or 9 days
213 (45.8%) after 5Z-7-oxozeaenol treatment compared with vehicle treatment (**Fig. 5A**). We next
214 performed a range of *in vitro* angiogenesis assays including cell viability, scratch migration, and tube
215 formation assay to test anti-angiogenic effects of 5Z-7-oxozeaenol in TIMEs and HRMECs. Since
216 TAK1 was found to protect endothelial cells from TNFα-induced apoptosis under inflammatory
217 conditions (*19*), we also evaluated the effect of 5Z-7-oxozeaenol on *in vitro* angiogenesis activity in
218 the presence or absence of TNFα. MTT assays revealed that TNFα alone did not affect the cell viability.
219 However, a profound reduction of cell viability was observed with cells treated with 5Z-7-oxozeaenol
220 or 5Z-7-oxozeaenol in the presence of TNFα stimulation compared with the control groups in TIMEs
221 and HRMECs, respectively. (**Fig. 5B and 5C**). Moreover, TNFα significantly reduced endothelial
222 migration by 20% (**Fig. 5D**). Cells treated with 5Z-7-oxozeaenol or TNFα/5Z-7-oxozeaenol showed
223 greater reductions in TIME migration of around 50% (**Fig. 5D**). Interestingly, TNFα alone did not
224 affect endothelial migration in HRMECs (**Fig. 5E**). 5Z-7-oxozeaenol resulted in a 20% reduction in
225 HRMEC migration both in the presence or absence of TNFα stimulation (**Fig. 5E**). Furthermore, 5Z-
226 7-oxozeaenol was effective at reducing TNFα-driven tube formation activity in TIMEs (**Fig. 5F**) and
227 HRMECs (**Fig. 5G**). No changes in tube formation activity were observed in 5Z-7-oxozeaenol-treated
228 TIMEs and HRMECs. Collectively, our data reveal that pharmacological inhibition of TAK1

229 significantly suppresses inflammation-mediated angiogenic signaling and reduces endothelial cell
230 angiogenic activity.
231
232 **Inhibition of TAK1 attenuates retinal neovascularization *in vivo***
233 To investigate the role of TAK1 in pathological neovascularization in the retina, we used a rat model
234 of oxygen-induced retinopathy (OIR) which yields ischemic avascular zones and preretinal
235 neovascularization similar to that observed clinically in PDR and retinopathy of prematurity. Neonatal
236 rats were subjected to daily cycles of 80% oxygen for 21 hours and ambient air for 3 hours from
237 postnatal day 0 (P0) to P14 to induce vaso-obliteration. At P14 rats were returned to room air, where
238 maximal preretinal neovascularization occured by P18, which was followed by a phase of vascular
239 regression (**Fig. 6A**). A significant increase in TAK1 expression at both RNA and protein levels was
240 observed in OIR retinae at P18 compared with controls (**Fig. 6B and 6C**). Examination of the retinal
241 distribution of TAK1 expression revealed that TAK1 expression was uniquely expressed in areas of
242 active neovascularization (**Fig. 6D**). To gain further insight into the role of TAK1 activation at the
243 peak of retinal neovascularization (P18), we then performed transcriptome analyses using bulk-RNA
244 sequencing. GSEA-based analysis revealed a positive enrichment of several TAK1 upstream pathways,
245 including IL1, TNF, TCR, BCR and TLR (**Fig. 6E and S16**), which is consistent with our findings in
246 patients with retinal neovascularization due to PDR. Similar to findings in humans, there was a
247 negative enrichment of genes associated with phototransduction and neuronal systems at P18 in the
248 rats. Of note, certain canonical pathways and biological processes related to angiogenesis were
249 positively enriched in the OIR model, such as VEGF-A/VEGFR2, PDGF pathway, the cellular
250 response to hypoxia, angiogenesis and inflammation (**Fig. 6E and S16**). Overall, our data implicates
251 active involvement of TAK1 in retinal neovascularization.
252 To assess whether intraocular application of a TAK1 inhibitor could be used to reduce retinal
253 neovascularization, 5Z-7-oxozeaenol was administered intravitreally to the OIR rats at P14 (**Fig. 7A**).
254 Four days after drug administration, retinal neovascularization was significantly suppressed by 51.3%
255 and 57.1% in OIR rats that had received low (18 ng) and high doses (90 ng) of 5Z-7-oxozeaenol,
256 respectively, compared to OIR rats that had vehicle only (**Fig. 7B and S17**). No significant difference
257 in retinal vaso-obliteration was found among these groups (**Fig. 7C**). We also examined the
258 development of deep capillary beds to assess the effects of TAK1 inhibition in physiological vessel
259 growth (*28*). Normal control rats developed a complete deep layer vasculature, while such
260 development was severely disrupted in OIR rats (**Fig. 7D**). We found that 5Z-7-oxozeaenol treatment
261 did not improve or damage the formation of deep capillary beds in OIR retina, which is likely attributed
262 to suppression of proliferative vessels by TAK1 inhibition. In addition to ICAM-1-related leukocyte

263 infiltration, microglia, the central nervous system resident immune cells, are also emerging as key
264 mediators or modulators of retinal inflammatory responses (*29*). Co-immunostaining of IB4 and Iba1
265 (marker of microglia) illustrated that 5Z-7-oxozeaenol treatment at both low and high doses
266 significantly attenuated the microglial adhesion to the vascular surface (**Fig. 8A and 8B**). Our data
267 also confirmed that TAK1 inhibition attenuated the expression of inflammatory and angiogenic signals,
268 TNFα, VEGFA and ICAM-1, in OIR retina (**Fig. 8C**).
269 Finally, we performed safety evaluations to test whether pharmacological TAK1 inhibition by
270 5Z-7-oxozeaenol adversely affects rodent retinae. The retinal whole mount results did not show any
271 abnormalities in the vasculature of P18 rats receiving vehicle or low or high dose of 5Z-7-oxozeaenol
272 under normoxic conditions (**Fig. S18**). Furthermore, electroretinography (ERG) and optical coherence
273 tomography (OCT) were performed to look for any retinal functional or structural changes in rats 28
274 days post intravitreal injection of high dose of 5Z-7-oxozeaenol. No difference in function was
275 observed for photoreceptors, bipolar cells or ganglion cells between vehicle- or 5Z-7-oxozeaenol-
276 treated eyes (**Fig. S19A-S19F**). No significant difference was observed in total retinal thickness or
277 thickness of various retinal layers including the nerve fiber layer (NFL) and outer retina layer (ORL)
278 between 5Z-7-oxozeaenol- and vehicle-treated eyes (**Fig. S19G and S19H**). Together, these results
279 suggested that intravitreal injection of 5Z-7-oxozeaenol does not result in adverse or toxic effects on
280 retinal function and structure up to 28 days post-injection.
281
282
283 **DISCUSSION**
284 TAK1 is a key modulator involved in a range of cellular functions including the immune response (*14*),
285 cell survival and death (*16*), angiogenesis (*20*), fibrosis (*30*) and tumor metastasis (*31*). TAK1 is
286 activated in response to various stimuli such as pro-inflammatory cytokines, hypoxia, oxidative stress,
287 metabolism, DNA damage, Wnt and osmotic shock (*14, 32-34*). Whether TAK1 is involved in
288 angiogenesis or inflammatory signaling in the retina, much less the molecular mechanisms by which
289 this occurs, has not been studied. Here, we show that TAK1 plays a central role in regulating
290 inflammatory and angiogenic signaling in the rat retina, and that the same signaling appears to be
291 involved in human diabetic retinopathy.
292 NFκB and MAPK are critical regulators of stress responses, immunity, inflammation and
293 angiogenesis. A variety of proinflammatory cytokines such as TNFα and IL1β activate these signaling
294 pathways through a common upstream kinase TAK1 (*35*). For instance, TNFα binds to its receptor 1
295 (TNFR1) upon inflammatory stimuli, triggering TAK1 that in complex with TAB1-3 phosphorylate

296 IKK at Ser[177] and Ser[181], which in turn leads to rapid proteasome-mediated degradation of the IκB
297 subunit. Subsequently, NFκB (p50/p65) is activated and translocated to the nucleus to promote gene
298 transcription (*17*). In addition, the TAK1 complex phosphorylates MAPKs to activate the JNK
299 pathway and the p38 MAPK pathways (both mediated by MKK4 and MKK7) as well as ERK by an
300 IKK2/tumor progression locus 2 (TPL2)-dependent pathway (*36*). Phosphorylation of p38 affects F-
301 actin polymerization in vascular endothelial cells and endothelial migration (*37*). Activation of JNK
302 and ERK subsequent to p21-activated kinase 1 stimulation promotes endothelial migration through
303 enhancement of cell motility (*38*). In particular, ERK is involved in VEGF-induced endothelial
304 proliferation, migration (via actin polymerization, lamellipodia and filopodia formation and myosin
305 contraction), morphogenesis (tube formation) and extracellular matrix degradation during
306 angiogenesis (*38*). In fact, deletion of TAK1 leads to the inactivation of both JNK and NFκB signaling,
307 as well as downregulation of expression of pro-survival genes in mice (*39*). Hence, deletion of TAK1
308 causes bone marrow and liver failure in mice due to the massive apoptotic death of hematopoietic cells
309 and hepatocytes, ultimately resulting in death within a few days. Moreover, endothelial-specific TAK1
310 knockout mice demonstrated intestinal and liver hemorrhage secondary to apoptosis of endothelial
311 cells and damaged vessels, resulting in rapid death (*19*). These data suggest that TAK1 protects
312 endothelial cells and maintains vascular integrity and homeostasis under inflammatory conditions.
313 Here, we provide the first evidence that both genetic and pharmacological inhibition of TAK1
314 activity in human endothelial cells prevents inflammatory stimuli from inducing sequential
315 phosphorylation of upstream kinases in both NFκB (p65) and MAPK (JNK, p38 and ERK) pathways
316 and suppressed expression of downstream genes that drive inflammation and angiogenesis, including
317 *ICAM-1*, *PTGS2*, *CXCL8* and *VEGF-A*. GSEA results confirmed that TAK1 knockout prevented TNFα
318 induced chemokine and cytokine activation predominantly through the NFκB pathway, which
319 attenuated inflammation and immune responses. Of note, GSEA did not identify significant changes
320 in the MAPK pathway in either wild type or TAK1-KO cells treated with TNFα, potentially because
321 the MAPK pathway activates more genes than the NFκB pathway (*40*) and fewer genes in MAPK
322 pathway showed significant changes compared to NFκB pathway. In addition, TAK1 inhibition by 5Z-
323 7-oxozeaenol significantly reduced endothelial cell angiogenic activities including migration,
324 proliferation and tube formation. These data together suggest a significant role for TAK1 in mediating
325 crosstalk between inflammatory and angiogenic pathways, both of which are crucial in pathological
326 angiogenesis.
327 TAK1 is thus a central regulator of cell survival and death (*16*). 5Z-7-oxozeaenol, a resorcylic
328 acid lactone derived from a fungus, acts as a potent and selective inhibitor of TAK1, which displays

329 more than 33- and 62-fold selectivity for TAK1 over binding of MEKK1 and MEKK4, respectively
330 (*27*). It forms a covalent complex with TAK1 and impedes both the kinase and ATPase activity of
331 TAK1 following bi-phase kinetics (*41*). We demonstrated that TAK1 inhibition by 5Z-7-oxozeaenol
332 directly reduced endothelial cell viability. This effect is more likely attributable to the suppression of
333 cell proliferation (such as cell cycle arrest, data not shown) rather than inducing cell apoptosis for we
334 did not observe any obvious morphologic changes associated with apoptosis in endothelial cells, such
335 as a decline in cell volume or aberrant cell nuclei (*42*). Intravitreal injection of 5Z-7-oxozeaenol
336 suppressed retinal neovascularization, and modulated elevated TNFα expression in the retina of OIR
337 rats, without causing degeneration of the normal vasculature. These data suggest that TAK1 inhibition
338 by 5Z-7-oxozeaenol may more specifically attenuate active angiogenesis with less risk of damage to
339 normal endothelial cells. However, further studies are required to understand the effects of repeated
340 5Z-7-oxozeaenol treatment. Moreover, TAK1 Inhibition by 5Z-7-oxozeaenol is known to block pro-
341 inflammatory signaling by selectively inhibiting TAK1 MAPKKK (*27*). In an animal model of early
342 brain injury, 5Z-7-oxozeaenol was shown to inhibit subarachnoid hemorrhage-induced
343 phosphorylation of p38 and JNK, the nuclear translocation of NFκB p65 and degradation of IκB,
344 ultimately reducing neuronal apoptosis and early brain injury (*43*). Similarly, another study
345 demonstrated that 5Z-7-oxozeaenol alleviated experimental autoimmune encephalomyelitis by
346 reducing the levels of pro-inflammatory cytokines in splenocytes and the central nervous system, thus
347 reducing the number of activated microglia and blocking p38 MAPK, JNK, and ERK signaling
348 pathways (*44*). Overactive microglia can damage surrounding cells, via a range of detrimental effects
349 including release of pro-inflammatory cytokines, reactive nitrogen species, reactive oxygen, and
350 proteolytic enzymes (*45*). We also observed diminished adhesion of microglia to endothelial cells in
351 OIR rats receiving 5Z-7-oxozeaenol treatment, suggesting that 5Z-7-oxozeaenol alleviates
352 inflammation in the retina, in part by reducing activation of microglia. Altogether, our results indicate
353 that TAK1 inhibition by 5Z-7-oxozeaenol suppresses ocular inflammation and neovascularization by
354 inhibiting cellular proliferation and microglia activation through NFκB and MAPK pathways.

355 5Z-7-oxozeaenol has been previously examined in a number of animal studies focusing on brain
356 injury (*46-48*). One study demonstrated that 5Z-7-oxozeaenol has neuroprotective function in a mouse
357 model of stroke (*46*). However, others suggest long-term TAK1 inhibition may not be protective in
358 neurodegenerative disorders (*49*). Chronic TAK1 inhibition resulted in apoptosis of a number of
359 normal cells, including keratinocytes, hepatocytes, and hematopoietic cells, raising safety concerns
360 (*39, 50, 51*). We demonstrated that TAK1 inhibition was capable of simultaneously reducing pro-
361 inflammatory cytokines and pro-angiogenic chemokines and growth factors in the retina of OIR rats.

362 In our studies, no adverse effects of intravitreal injection of the TAK1 inhibitor on retinal function or
363 structure were apparent up to 28 days post-injection. Specifically, TAK1 inhibition by intravitreal
364 injection of 5Z-7-oxozeaenol did not affect the scotopic threshold response, a highly sensitive
365 electroretinography measure of retinal ganglion cell activity (*52*). Another study has shown that
366 systemic TAK1 inhibition by 5Z-7-oxozeaenol preserved β cell function, thus improving overall health
367 condition in the animal with autoimmune diabetes (*53*). It is worth noting that 5Z-7-oxozeaenol may
368 have off-target effects, potentially stemming from cross-reactivity with other human kinases that
369 possess an analogous cysteine (*54*). Whilst encouraging, further studies with chronic dosing of 5Z-7-
370 oxozeaenol are clearly needed to confirm safety.
371 In summary, the present study identifies TAK1 as a mediator of inflammatory and angiogenic
372 signaling pathways, with a central role in retinal neovascularization. We demonstrated elevated TAK1
373 expression in both human and rat retinae associated with neovascularization. We showed that reducing
374 TAK1 suppressed angiogenic activities *in vitro* through NFκB signaling pathway. Using 5Z-7-
375 oxozeaenol, a well-studied selective TAK1 inhibitor, we demonstrated that pharmacological inhibition
376 of TAK1 can effectively suppress angiogenesis in both *ex vivo* and *in vivo* models in rats. These
377 findings provide new insights into the molecular and cellular mechanisms by which TAK1 modulates
378 inflammation and angiogenesis, thus highlighting a potential alternative approach to anti-VEGF
379 treatment to prevent pathological retinal neovascularization.
380
381
382

383 **MATERIALS AND METHODS**

384 **Data accession**

385 To assess TAK1 expression in human retinal cells, we utilized data single cell transcriptomes from
386 human retina, from the Gene Expression Omnibus
387 (https://www.ncbi.nlm.nih.gov/geo/query/acc.cgi?acc=GSE135133) (accessed on September 20,
388 2020).

389 To access gene expression in retinas from patients with retinal neovascularization due to
390 proliferative diabetic retinopathy, we obtained the RNA-seq raw counts and TPM matrices from the
391 Gene Expression Omnibus (https://www.ncbi.nlm.nih.gov/geo/query/acc.cgi?acc=GSE102485)
392 (accessed on September 27, 2020). We specifically compared samples from patients with retinal
393 neovascular proliferative membranes due to type II diabetes (GSM2739349, GSM2739350 and
394 GSM2739351) and those from normal controls (GSM2739364, GSM2739365 and GSM2739366).

395

396 **scRNA-seq data analysis**

397 scRNA-seq data were retrieved from a public dataset (GSE135133) and analyzed in R (v3.6.3) using
398 Seurat (v3.2) (*55, 56*) with customized scripts. In brief, cell identity was assigned according to the
399 assignment labels kindly provided by the authors after we normalized and scaled all human samples.
400 We assigned ganglion cells, horizontal cells, bipolar cells, amacrine cells, cones and rods as the neural
401 cells while immune cells, basal cells, red cells, pericytes, endothelial cells, astrocytes and Müller cells
402 were regarded as non-neural cells. Dot plots were utilized for visualization of gene expression levels
403 and percentage difference for various cell types.

404

405 **RNA isolation**

406 Total cells or tissue RNA was isolated using Zymo Quick-RNA MiniPrep kit (R1055; Zymo Research,
407 Irvine, CA) according to the manufacturer's instructions. The quantity of RNA was evaluated with a
408 NanoDrop ND-1000 spectrophotometer (NanoDrop Technologies, Wilmington, DE).

409

410 **RNA-seq analysis**

411 Analysis was undertaken in triplicate on total RNAs (1 μg) from normoxic and OIR rats at P14,
412 prepared as per the manufacturers' instructions. cDNA libraries were sequenced by using an Illumina
413 Hiseq-2500 RNA-seq platform as 50 bp single end chemistry at the Australian Genome Research
414 Facility (AGRF, Melbourne, VIC, Australia). The raw fastq files of single-end reads were removed
415 the adapter sequences and the low-quality reads were dropped by Trimgalore 0.4.4 (Babraham

416 Bioinformatics). Filtering parameter were set as follow: -q 25 --length 50 -e 0.1 --stringency 5. The
417 trimmed reads were subjected to alignment with default setting using STAR 2.5.3. The reference
418 genomes for human and rat were hg38 and rn6, respectively. Aligned RNA-seq data was counted over
419 gene exon using feature Counts (subread 1.6.4). Genes were annotated as per the Gencode Version 33
420 annotation file.
421
422 **Gene set enrichment analysis (GSEA)**
423 GSEA was run on the human dataset of protein-coding genes in PDR versus controls and on the rodent
424 dataset of protein-coding genes in OIR versus controls, against canonical pathway genesets collection
425 (c2.cp.v7.2, Broad Institute) by using 1000 genesets permutations. Only genesets with FDR < 0.05
426 were considered. Readcount values were loaded into R (v3.6.3) for statistical analysis and the heatmap
427 function was used to perform hierarchical clustering analysis and for data representation.
428
429 **Quantitative polymerase chain reaction (qPCR)**
430 Total RNAs (100 ng) was reverse transcribed to cDNA using a High-Capacity cDNA Reverse
431 Transcription kit (4368814; Life Technologies, Carlsbad, CA). Quantitative PCR was performed using
432 TaqMan fast advanced master mix (4444553; Applied Biosystems, Foster City, CA) and gene TaqMan
433 probe sets to detect gene expression (**Table S1**). The expression levels of target genes were normalized
434 to the levels of rat beta-actin (Rn00821065_g1) or human GAPDH (Hs99999905_m1). Subsequently,
435 the ΔΔCt method was used to evaluate relative expression level (fold change) in each condition versus
436 the corresponding control condition.
437
438 **Cell culture**
439 Telomerase-immortalized human microvascular endothelial cell (TIME; CRL-4025™) and primary
440 human retinal microvascular endothelial cell (HRMEC; ACBRI 181V) were purchased from American
441 Type Culture Collection (ATCC; Manassas, VA) and Cell Systems (Kirkland, WA). Endothelial cells
442 were cultured in EBM™ Plus Basal Medium supplied with EGM™ Plus SingleQuots™ supplements
443 (CC-5035; Lonza, Basel, Switzerland). All cell lines were maintained in a humidified incubator at
444 37°C and 5% CO_2. Cell lines were mycoplasma free tested by MycoAlert™ Mycoplasma Detection
445 Kit (LT07; Lonza).
446
447 **Western blotting**
448 A standard immunoblotting protocol was used. Briefly, protein was extracted from cells or retinas with
449 Pierce RIPA buffer (89900; Life Technologies) supplied with protease inhibitor cocktail

450 (11697498001; Roche Diagnostics, Basel, Switzerland). Equal amounts of cell lysates from different
451 groups were subjected to Western blotting analysis with specific antibodies against IκB, phospho-
452 NFκB p65, NFκB p65, phospho-p44/42 MAPK (Erk1/2), p44/42 MAPK (Erk1/2), phospho-TAK1,
453 TAK1, phospho-SAPK/JNK, SAPK/JNK, phospho-p38 MAPK, p38 MAPK (4814, 3033, 4764, 9101,
454 4695, 9339, 4505, 9255, 9252, 9211, 8690, respectively; Cell Signaling), and β-actin (MAB1501;
455 Merck Millipore, Burlington, MA). The quantitative densitometry was analyzed using Image Pro Plus
456 software (Media Cybernetics, Rockville, MA).
457
458 **Aortic ring assay**
459 The aortic ring assay was performed as previously described (*57*). Briefly, aortae were removed from
460 euthanized C57BL/6 mice and immediately transferred to a culture dish containing ice-cold
461 EBM™ Plus Basal Medium supplied with EGM™ Plus SingleQuots™ supplements (Lonza).
462 Peripheral fibroadipose tissue was carefully removed. Aortae were sectioned into rings ~1 mm in width.
463 Each aortic ring was placed in an individual well covered with 120 µl Matrigel™ Basement Membrane
464 Matrix and immersed in 200 µl complete medium with or without 5Z-7-oxozeaenol (1 µM, Tocris
465 Bioscience, Bristol, UK) for 9 days in a 48-well plate. The medium was refreshed and 5Z-7-oxozeaenol
466 was replenished every 3 days. Images of individual explants were taken from day 0 to day 9.
467 Neovascular sprouting area was quantified with Adobe Photoshop Elements 13.
468
469 **Cell viability assay**
470 Cell viability was measured by colorimetric 3-(4,5-dimethylthiazol-2-yl)-2,5-diphenyl-2H-tetrazolium
471 bromide (MTT) (M2128; Sigma-Aldrich, St Louis, MI) assay. Briefly, TIMEs or HRMECs were
472 seeded into 96-well plates at a density of 5×10^3 per well. Cells were treated with 5Z-7-oxozeaenol (1
473 µM) in the presence or absence of TNF-α (10 ng/ml) for 48 hours on the following day. Cells were
474 then treated with 10 µl MTT (5.5 mg/ml) and incubated for 1 hour. After removal of the medium, cells
475 were lysed in 100 µl DMSO (D8418; Sigma-Aldrich) and absorbance values were measured using a
476 Spark® Multimode Microplate Reader at 550 nm (Tecan; Männedorf, Switzerland).
477
478 **Cell migration assay**
479 TIMEs or HRMECs were seeded at a density of 4×10^4/well in a 96-well plate. A wound to the cell
480 monolayer was made using an Incucyte® 96-well WoundMaker Tool (4563; Incucyte, Ann Arbor, MI),
481 creating an incision-like gap. After removing debris-containing medium, cells were washed with 100
482 µl PBS. Cells were then exposed to 5Z-7-oxozeaenol (1 µM) with or without TNF-α (10 ng/ml) in 100
483 µl serum/growth factor-free medium containing VEGF (20ng/ml) (293-VE-010; R&D Systems,

484 Minneapolis, MN). The scratch area was photographed using an Incucyte® Live-Cell Imaging and
485 Analysis System (Incucyte) immediately after wounding (0 hour) and 16 hours post-wounding. The
486 scratch area was quantified using ImageJ version 1.48 software (http://imagej.nih.gov/ij/). Cell
487 migration was expressed as a percentage of closure of the scratch area: (scratch area at 0 hour - scratch
488 area at 16 hour) / scratch area at 0 hour × 100%.
489
490 **Endothelial tube formation assay**
491 Endothelial tube formation was quantified as previously described (*58*). In brief, TIMEs or HRMECs
492 were seeded at a density of 2×10^5/well in a 6-well plate. Cells were then pre-treated with 5Z-7-
493 oxozeaenol (1 μM) for 0.5 hours followed by TNF-α (10 ng/ml) treatment for 24 hours. A 96-well
494 plate was pre-coated with 50 μl Matrigel™ Basement Membrane Matrix (356234; Corning) and
495 incubated at 37°C for at least 15 minutes to allow Matrigel polymerization. Conditioned endothelial
496 cells were trypsinized and seeded at a density of 3×10^4 in pre-coated 96-well plates in 100 μl
497 serum/growth factor-free medium containing VEGF (20ng/ml). Each condition was tested with three
498 replicates. Images were photographed using an Incucyte® Live-Cell Imaging and Analysis System at
499 defined time points. Endothelial mesh numbers were quantified by the ImageJ (version 1.48) installed
500 with Angiogenesis Analyzer Plugin.
501
502 **Animals**
503 Pregnant Sprague-Dawley rats (female, 12-14 weeks old) and Brown Norway rats (male, 12 weeks
504 old) were supplied by the Animal Resources Centre (Murdoch, WA, Australia) and Cambridge Farm
505 Facility of the University of Tasmania (Cambridge, TAS, Australia). Animals were housed in standard
506 cages with a temperature/humidity-controlled and a 12-hour light (50 lux illumination)/12-hour dark
507 (<10 lux illumination) cycle environment. Food and water were available *ad libitum*. All animal
508 experiments were conducted in accordance with guidelines of the ARVO Statement for the Use of
509 Animals in Ophthalmic and Vision Research and were approved by the Animal Ethics Committees of
510 St Vincent's Hospital (004/16), the University of Melbourne (13-044UM), and the University of
511 Tasmania (A0017311). Rats were randomly allocated to treatment groups such that littermates were
512 distributed equally between groups.
513
514 **Rat model of oxygen-induced retinopathy and intravitreal injection of 5Z-7-oxozeaenol**
515 The oxygen-induced retinopathy model was induced in rats as previously described (*59*). Briefly,
516 Sprague-Dawley litters (within 12 hours of birth; P0) and their nursing mothers were exposed to daily
517 cycles of 80% O_2 for 21 hours and room air for 3 hours in a custom-built and humidity-controlled (<

518 80%) chamber until P14. At P14 animals were returned to room air until P16 or P18, when they were
519 sacrificed to harvest retinae. An ProOx 110 oxygen controller (BioSpherix; Parish, NY) was used to
520 regulate and monitor the oxygen level. At P14, intravitreal injections were performed to administer
521 5Z-7-oxozeaenol visualizing with a microsurgical microscope. Under surface anesthesia, a puncture
522 in the superior temporal quadrant of the limbus was made by a 30-gauge needle. A hand-pulled glass
523 micropipette (Bio-Strategy, Australia) connected to a 10 µl Hamilton syringe (Hamilton Company,
524 Reno, NV) was inserted into the vitreous cavity, and one microliter of balanced salt solution containing
525 1% DMSO (as vehicle), low (18 ng) or high dose (90 ng) of 5Z-7-oxozeaenol was intravitreally
526 injected into the eye. For safety evaluation, Brown Norway rats were intravitreally injected with 1 µl
527 high dose (90 ng) of 5Z-7-oxozeaenol or vehicle. Eyes were excluded from the study if large backflow
528 after injection or severe hemorrhage were occurred. Electroretinography and optical coherence
529 tomography imaging evaluation was undertaken 28 days post-intravitreal injection in anesthetized
530 animals as previously described (*60*).
531
532 **Immunohistochemistry and vessel quantification**
533 Collection of donor samples was approved by the Human Research Ethics Committee of the Royal
534 Victorian Eye and Ear Hospital (HREC13/1151H) and carried out in accordance with the approved
535 guidelines. Post-mortem eye globes were obtained via the Lions Eye Donation Service (Royal
536 Victorian Eye and Ear Hospital, East Melbourne, VIC, Australia) and processed for paraffin
537 embedding and sectioning following standard histological procedures. Briefly, donated eyes were
538 isolated, fixed, and permeabilized. The cross sections were stained with anti-TAK1 (1:100; NBP1-
539 87819, Novus Biologicals, Littleton, CO) and anti-CD31 (1:25; M0823, DAKO, Jena, Germany)
540 primary antibody and then with the appropriate secondary antibodies. Images were digitized using a
541 confocal laser scanning microscope (FV3000; Olympus, Tokyo, Japan).
542 The rat retinal flat-mount were collected at P18 followed by retina dissection, staining overnight
543 with isolectin GS-IB$_4$ Alexa Fluor™ 488 conjugate (5 µg/mL; I21411, Life Technologies), anti-TAK1
544 (1:100; NBP1-87819, Novus Biologicals), or anti-Iba1 (1:300; 019-19741, FUJIFILM Wako
545 Chemicals, Richmond, VA), and then incubated with the appropriate secondary antibodies. The images
546 were captured by FV3000 confocal laser scanning microscope. The avascular (vaso-obliteration) and
547 neovascularized areas were quantified by two blinded assessors using Adobe Photoshop (San Jose,
548 CA) (*61*). Deep vessel area was analyzed by AngioTool software (National Institutes of Health,
549 Bethesda, MA) (*62*).
550
551 **Statistical analysis**

552 All data are expressed as mean ± SEM. Statistical analyses were performed with Graphpad Prism 7
553 (GraphPad, San Diego, CA) using student t-test for unpaired data, one-way or two-way ANOVA
554 wherever appropriate followed by Tukey's or Bonferroni's multiple comparisons test. P values < 0.05
555 were considered statistically significant.
556
557 **Data and resource availability statement**
558 The main datasets generated or analyzed during this study are included here in the article. Retinal RNA
559 profiles of OIR and control rats have been deposited in Gene Expression Omnibus and are accessible
560 through GEO Series accession number GSE104588
561 (https://www.ncbi.nlm.nih.gov/geo/query/acc.cgi?acc= GSE104588). The original Western Blot
562 images and the details of statistical analysis for this study are available in the supplementary
563 information. Other original datasets will also be available to the research community upon reasonable
564 request.

ACKNOWLEDGEMENTS

The authors thank UTAS CFF animal technicians, Karen Shiels, Keri Smith, Heather Howard, Lisa Harding and Danielle Eastley for their assistance with rat chamber operation. We also thank Dr Jacqueline Y.K. Leung for assistance with intravitreal injection, and Zheng He for assistance with retinal imaging. This work was supported by grants from the National Health and Medical Research Council of Australia (1061912, 1185600 and 1123329), the Ophthalmic Research Institute of Australia, the National Natural Science Foundation of China (#82000902) and the Shenzhen Key Laboratory of Biomimetic Materials and Cellular Immunomodulation (ZDSYS20190902093409851). GJD was a Principal Research Fellow of NHMRC. The Centre for Eye Research Australia receives Operational Infrastructure Support from the Victorian Government.

COMPETING INTERESTS

The authors have declared that no competing interest exists.

AUTHOR CONTRIBUTIONS

Conceptualization- F-L.L., J-H.W., P.vW., G.J.D., G-S.L. Methodology- F-L.L., C.M., J-H.W., B.V.B., P.vW., G-S.L. Formal Analysis- F-L.L., J-H.W., J.C., R.C.B.W., B.V.B., G-S.L. Investigation- F-L.L., J-H.W., J.C., L.Z., Y-F.C., L.T., C.M., S.L., D.L., C-L.T., B.V.B. Resources- R.C.B.W., A.W.H., C-L.T., G.J.D., P-Y.W., G-S.L. Data Curation- F-L.L., J-H.W., J.C., G-S.L. Writing (Original Draft)- F-L.L., J-H.W., G-S.L. Writing (Review & Editing)- J.C., C.M., R.C.B.W., B.V.B., P.vW., G.J.D., P-Y.W. Project Administration- F-L.L., J-H.W., G-S.L. Funding Acquisition- L.T., G.J.D., P-Y.W., G-S.L. Project Supervision- G.S.L.

589 **TABLE**

590 **Table 1** Effects on selected major biological functions and genes mediated by NFκB signaling in TAK1-KO/TNFα data set compared to TIME
591 WT/TNFα or human proliferative diabetic retinopathy data set.

592

GENE NAME	WT vs WT TNFα (TIME)		TAK1-KO vs TAK1-KO TNFα (TIME)		Control vs PDR (human)	
	log2FoldChange	**FDR**	**log2FoldChange**	**FDR**	**log2FoldChange**	**FDR**
Cytokines/chemokines and their modulators						
IL32	2.885075068	8.07E-24	2.43768644	2.60E-08	7.337923821	5.45E-09
EBI3	6.198904072	7.52E-14	3.007982959	0.023249158	NS	NA
IL1B	4.356722201	3.94E-11	ND	NA	6.951689055	0.001062874
CXCL1	1.837107209	7.24E-11	1.706754297	0.023249158	7.247441268	2.79E-08
IL1A	3.298057395	5.17E-10	1.666059481	6.69E-05	NS	NA
IL4I1	4.274123628	1.64E-08	1.97340997	1.70E-05	NS	NA
CCL2	4.79431389	2.35E-08	4.47501059	0.001053927	4.701240948	6.98E-05
CCL5	6.50100412	1.47E-07	0.575490181	NS	6.831728049	3.77E-07
CXCL2	2.68971782	8.93E-07	1.355595731	0.036825723	8.145999314	8.23E-08
CXCL6	3.200455586	1.13E-05	ND	NA	NS	NA
CXCL8	3.400950627	2.62E-05	2.170922901	0.00249688	10.82611594	2.20E-10
CXCL10	9.884759997	6.15E-05	ND	NA	9.751163405	7.68E-08
CXCL11	8.862329366	0.000107195	ND	NA	NS	NA
IL12RB1	2.384477086	0.000159695	2.519724934	0.003026935	NS	NA
IFNGR2	1.067233203	0.000220676	-0.010609023	NS	3.704272794	2.17E-06
CX3CL1	4.934119032	0.000299947	ND	NA	NS	NA
CCL20	5.98071708	0.000308261	ND	NA	NS	NA
LTB	5.023062961	0.000803449	ND	NA	3.438844059	2.36E-05

IL15RA	0.950048019	0.001276256	0.315621103	NS	NS	NA
IL12A	1.681737512	0.030734062	ND	NA	NS	NA
IL15	0.850427352	0.031624223	0.510248295	NS	3.131434431	0.006648566
Cell adhesion molecules						
ICAM1	3.581426072	4.18E-07	1.309385377	0.031159341	8.875807897	3.85E-05
VCAM1	10.39066838	6.70E-07	ND	NA	3.587214659	0.002361912
TNC	1.727069145	5.30E-05	0.434407509	NS	6.13710052	1.36E-06
CD44	0.583552057	1.02E-02	1.03652987	5.69E-07	4.438643898	6.11E-16
NEXN	-1.099912175	1.33E-02	-0.227113467	NS	NS	NA
Stress response						
MX1	3.669808687	5.89E-08	1.314998701	NS	3.098000727	0.000335443
SOD2	3.408334795	0.000224549	0.479507031	NS	2.298829823	0.015254884
PTGS2	1.768472879	0.006173644	0.547609304	NS	7.44888707	1.59E-07
Growth factors, ligands and their modulators						
FSTL3	1.179795988	9.17E-10	0.928605483	1.72E-09	4.291636096	0.002125552
VEGFC	1.727333267	1.06E-09	0.840157924	NS	3.212454719	0.018991682
PDGFB	1.054284963	2.71E-06	0.020068321	NS	5.289508792	0.002421184
SPP1	-1.764501485	3.64E-06	-1.674569805	0.009011623	-2.761477405	0.000452176
CSF1	1.540479441	9.12E-05	0.325643321	NS	4.612793613	0.000377798
VEGFA	0.978149971	0.000290817	0.495025602	0.003932897	NS	NA
BDNF	-0.796191579	0.002934927	-0.746511425	0.016139526	NS	NA
BMP2	1.542956691	0.003265102	0.592970121	NS	2.427699141	0.00010727
TGFBR1	0.700409513	0.021957163	0.313969523	0.035887655	3.884136817	0.000675247
PDGFA	0.705182729	0.045217876	0.310168524	0.018563222	NS	NA
Regulators of apoptosis						

TNFAIP3	2.287391903	3.76E-07	1.956586566	0.001122203	2.58343034	0.020845273
CASP1	1.338748263	0.000195795	0.115336995	NS	5.958734923	6.10E-09
XAF1	8.669201677	0.000965032	ND	NA	NS	NA
TNFAIP8	1.208463108	0.008518801	0.576531682	0.037959056	4.362835999	9.89E-05
BID	0.724938967	0.017590667	0.263745692	0.017317211	3.002199987	3.21E-07
NUAK2	2.334300335	0.022201413	1.522911528	0.000103276	NS	NA

NA: Not Available, ND: Not Detected, NS: Not Significant, PDR: Proliferative Diabetic Retinopathy, FDR: False Discovery Rate.

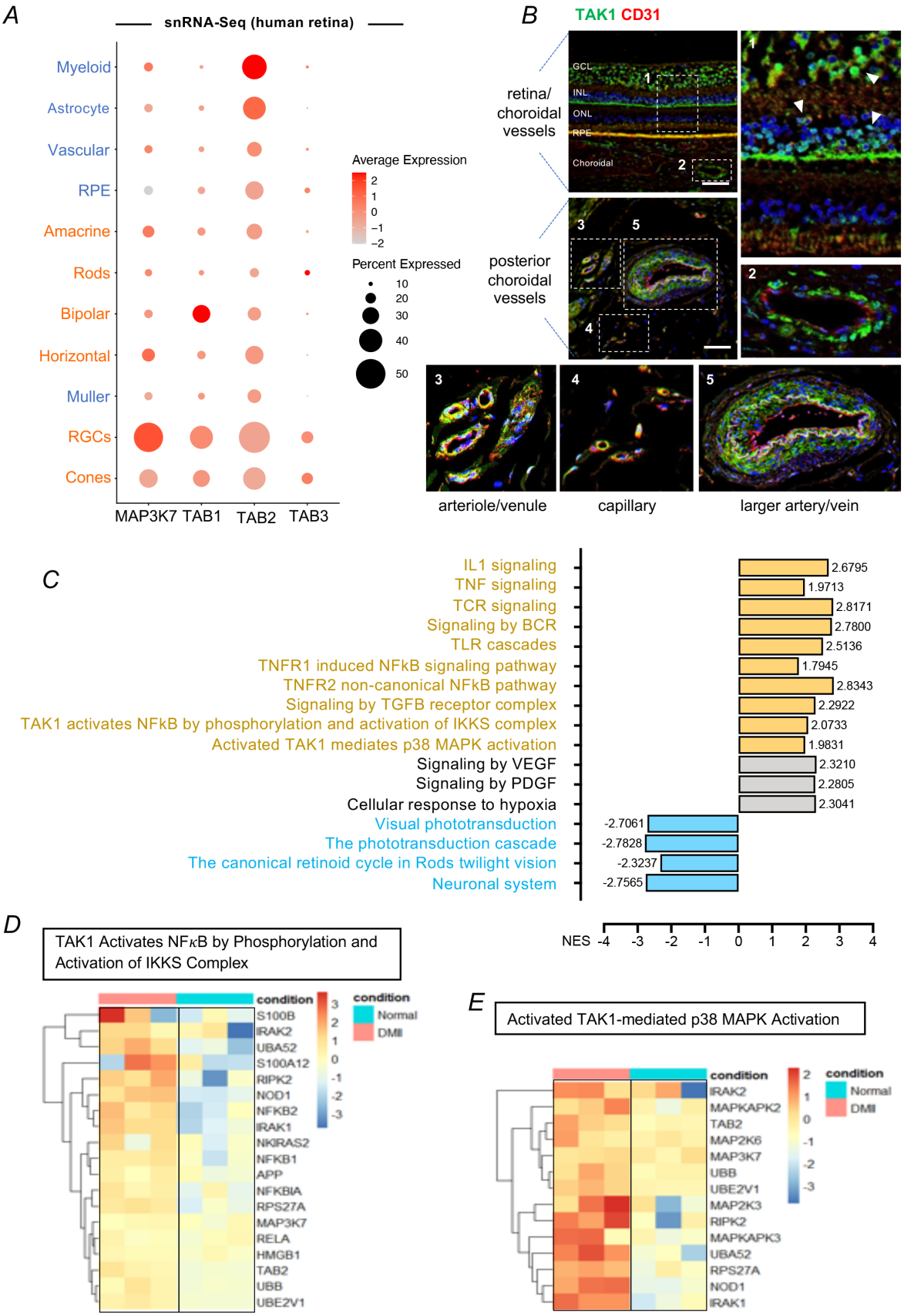
A
snRNA-Seq (human retina)
Myeloid
Astrocyte
Vascular
RPE
Amacrine
Rods
Bipolar
Horizontal
Muller
RGCs
Cones
MAP3K7 TAB1 TAB2 TAB3
Average Expression
Percent Expressed
B
TAK1 CD31
retina/ choroidal vessels
posterior choroidal vessels
GCL
INL
ONL
RPE
Choroidal
arteriole/venule
capillary
larger artery/vein
C
IL1 signaling 2.6795
TNF signaling 1.9713
TCR signaling 2.8171
Signaling by BCR 2.7800
TLR cascades 2.5136
TNFR1 induced NFkB signaling pathway 1.7945
TNFR2 non-canonical NFkB pathway 2.8343
Signaling by TGFB receptor complex 2.2922
TAK1 activates NFkB by phosphorylation and activation of IKKS complex 2.0733
Activated TAK1 mediates p38 MAPK activation 1.9831
Signaling by VEGF 2.3210
Signaling by PDGF 2.2805
Cellular response to hypoxia 2.3041
Visual phototransduction -2.7061
The phototransduction cascade -2.7828
The canonical retinoid cycle in Rods twilight vision -2.3237
Neuronal system -2.7565
NES -4 -3 -2 -1 0 1 2 3 4
D
TAK1 Activates NFκB by Phosphorylation and Activation of IKKS Complex
condition
Normal
DMII
S100B
IRAK2
UBA52
S100A12
RIPK2
NOD1
NFKB2
IRAK1
NKIRAS2
NFKB1
APP
NFKBIA
RPS27A
MAP3K7
RELA
HMGB1
TAB2
UBB
UBE2V1
E
Activated TAK1-mediated p38 MAPK Activation
condition
Normal
DMII
IRAK2
MAPKAPK2
TAB2
MAP2K6
MAP3K7
UBB
UBE2V1
MAP2K3
RIPK2
MAPKAPK3
UBA52
RPS27A
NOD1
IRAK1

595

596 **Fig. 1 Characterization of TAK1 expression in patients with retinal neovascularization**
597 **associated with proliferative diabetic retinopathy in humans.**
598 (A) Single nuclei RNAseq (snRNAseq) characterization of TAK1 (MAP3K7) expression in normal
599 human retina. TAK1 and TAK1-associated proteins (TAB1-3) were expressed in most neural (red)
600 and non-neural (blue) cells in the retina, including cell associated with the retinal vasculature. (B)
601 Characterization of TAK1 expression in the normal human retina. Endothelial cells were labelled with
602 CD31 (red) and counterstained with TAK1 (green) in retinal section. Apart from neural cells, TAK1
603 expression was also found in vascular endothelial cells, especially in retinal capillaries (3 and 4). Scale
604 bar: 100 μm. (C) Gene-set enrichment analysis (GSEA) indicated that TAK1 upstream pathways
605 including IL1, TNF, TCR, BCR, TLR, TNFR, or TGFβ signaling (Reactome Pathway Database) were
606 positively enriched in retinal samples from patients with retinal neovascularization due to proliferative
607 diabetic retinopathy. Engagement of TAK1-activated NFκB and p38 MAPK pathways and negative
608 impact of on retinal neural functions were also identified. (D) Heatmap illustration of genes involved
609 in TAK1-NFκB and TAK1-p38 MAPK pathways in the retina of eyes with proliferative diabetic
610 retinopathy. GCL: ganglion cell layer; INL: inner nuclear layer; ONL: outer nuclear layer; RPE: retinal
611 pigment epithelium.
612
613

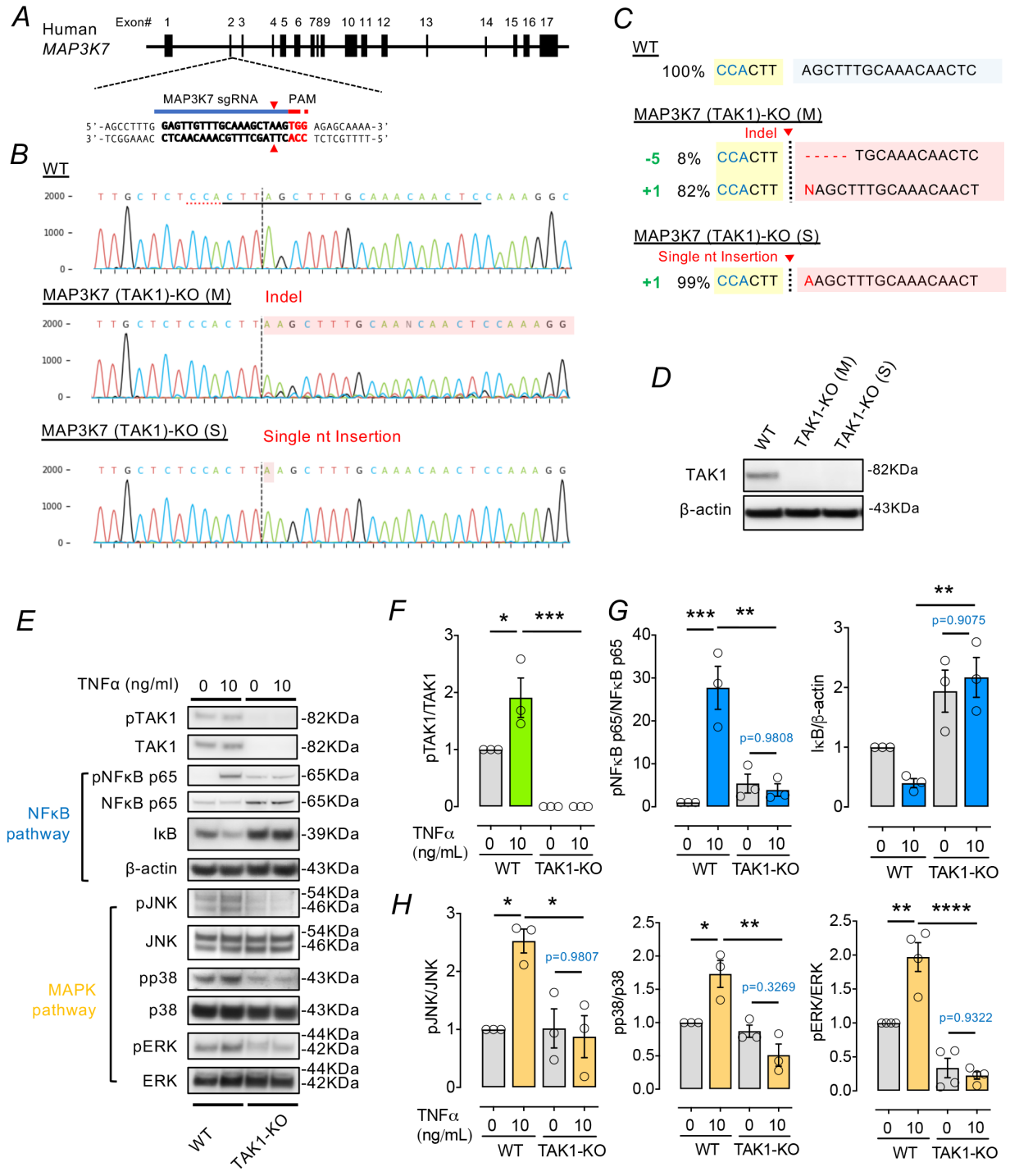

Fig. 2 CRISPR/Cas9-mediated TAK1 knockout impaired NFκB and MAPK pathways and downstream pro-inflammatory/pro-angiogenesis gene expressions in human endothelial cells. (A) Genome of TAK1 (MAP3K7). A sgRNA was designed to target exon 2 of the TAK1 gene. (B) As compared with wild type (WT) TIMEs, genomic DNA sequences revealed a heterogeneous MAP3K7 knockout (KO) (M) and a single homogenous MAP3K7 KO (S) TIMEs were established after CRISPR editing. (C) Sanger sequencing confirmed that MAP3K7 KO (M) TIMEs had mixed indel profiles, and

621 MAP3K7 KO (S) TIMEs was a single nucleotide insertion, which created as premature Stop Condon
622 in TAK1 exon 2 region. (D) Western blot characterization of TAK1 knockout in MAP3K7 KO (M)
623 and MAP3K7 KO (S) TIMEs. (E) Wild type (WT) and TAK1 knockout (TAK1-KO) TIME cells were
624 stimulated by TNFα (10 ng/ml) for 10 minutes. Activation of TAK1, NFκB p65, IκB, JNK, p38, and
625 ERK assessed using western blot (n = 3-4). Genetic TAK1 deletion reduced TAK1 expression and
626 impaired (G) NFκB (NFκB p65 and IκB) and (H) MAPK (p38, JNK, and ERK) signaling in TIME
627 cells treated with TNFα. All data were expressed as means ± SEM. Statistical analysis was undertaken
628 with one-way ANOVA and Tukey's multiple comparison test; *$P < 0.05$, **$P < 0.01$, ***$P < 0.001$,
629 ****$P < 0.0001$.
630
631

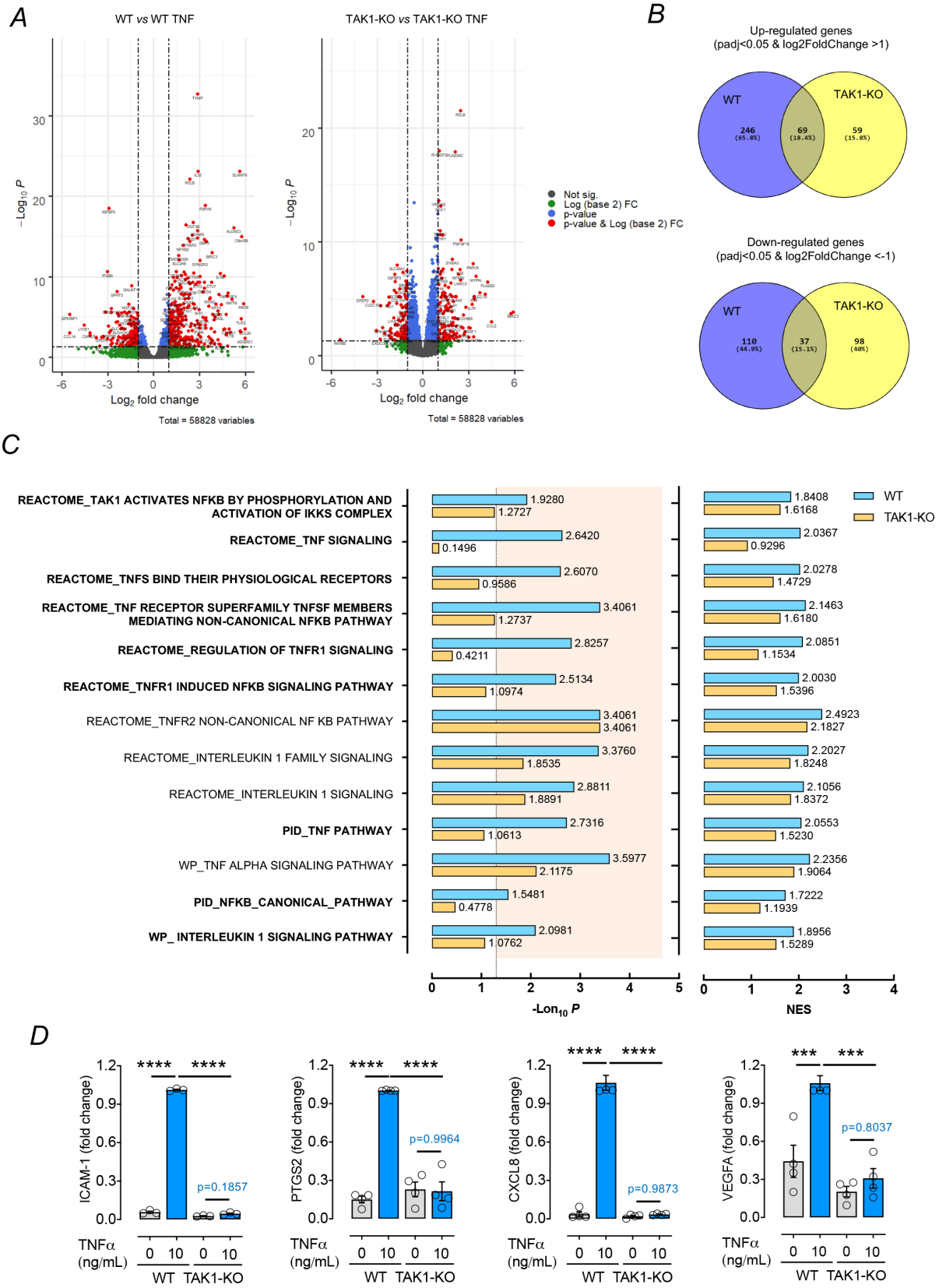
A
WT vs WT TNF
TAK1-KO vs TAK1-KO TNF
−Log10 P
Log2 fold change
Total = 58828 variables
Not sig.
Log (base 2) FC
p-value
p-value & Log (base 2) FC
B
Up-regulated genes
(padj<0.05 & log2FoldChange >1)
WT
TAK1-KO
246 (65.8%)
69 (18.4%)
59 (15.8%)
Down-regulated genes
(padj<0.05 & log2FoldChange <-1)
110 (44.9%)
37 (15.1%)
98 (40%)
C
REACTOME_TAK1 ACTIVATES NFKB BY PHOSPHORYLATION AND ACTIVATION OF IKKS COMPLEX
REACTOME_TNF SIGNALING
REACTOME_TNFS BIND THEIR PHYSIOLOGICAL RECEPTORS
REACTOME_TNF RECEPTOR SUPERFAMILY TNFSF MEMBERS MEDIATING NON-CANONICAL NFKB PATHWAY
REACTOME_REGULATION OF TNFR1 SIGNALING
REACTOME_TNFR1 INDUCED NFKB SIGNALING PATHWAY
REACTOME_TNFR2 NON-CANONICAL NF KB PATHWAY
REACTOME_INTERLEUKIN 1 FAMILY SIGNALING
REACTOME_INTERLEUKIN 1 SIGNALING
PID_TNF PATHWAY
WP_TNF ALPHA SIGNALING PATHWAY
PID_NFKB_CANONICAL_PATHWAY
WP_ INTERLEUKIN 1 SIGNALING PATHWAY
WT
TAK1-KO
-Lon10 P
NES
D
ICAM-1 (fold change)
PTGS2 (fold change)
CXCL8 (fold change)
VEGFA (fold change)
****
***
p=0.1857
p=0.9964
p=0.9873
p=0.8037
TNFα (ng/mL)
WT TAK1-KO

632

633 **Fig. 3 TAK1 knockout prevents TNFα-induced inflammatory cascade through the NFκB**
634 **pathway in human endothelial cells.**
635 (A) Volcano plots show genes that were significantly changed in both wild type and TAK1-KO TIME
636 cells when stimulated by TNFα. Red dots refer to genes showing a log2|fold change| > 1 and FDR <
637 0.05. Labels indicate significantly up-regulated genes in each data set. (B) The Venn diagrams shows
638 altered genes in WT TNFα (WT TNFα set) and TAK1-KO TNFα transcriptomes (TAK1-KO TNFα
639 set). The 246 and 110 genes were exclusively up-regulated and down-regulated in WT TNFα set and
640 not in the TAK1-KO TNFα set. (C) GSEA results showed inflammation-related pathways, such as
641 NFκB, TNF and IL1 signaling, were positively enriched in cells stimulated by TNFα, while TAK1-
642 KO suppressed those pathways. (D) TAK1 knockout significantly inhibited expression of *ICAM-1*,
643 *PTGS2*, *CXCL8*, and *VEGFA* in cells stimulated by TNFα for 24 hours. Data are shown as means ±
644 SEM. Statistical analysis was undertaken with one-way ANOVA and Tukey's multiple comparison
645 test; ***$P < 0.001$, ****$P < 0.0001$.
646
647

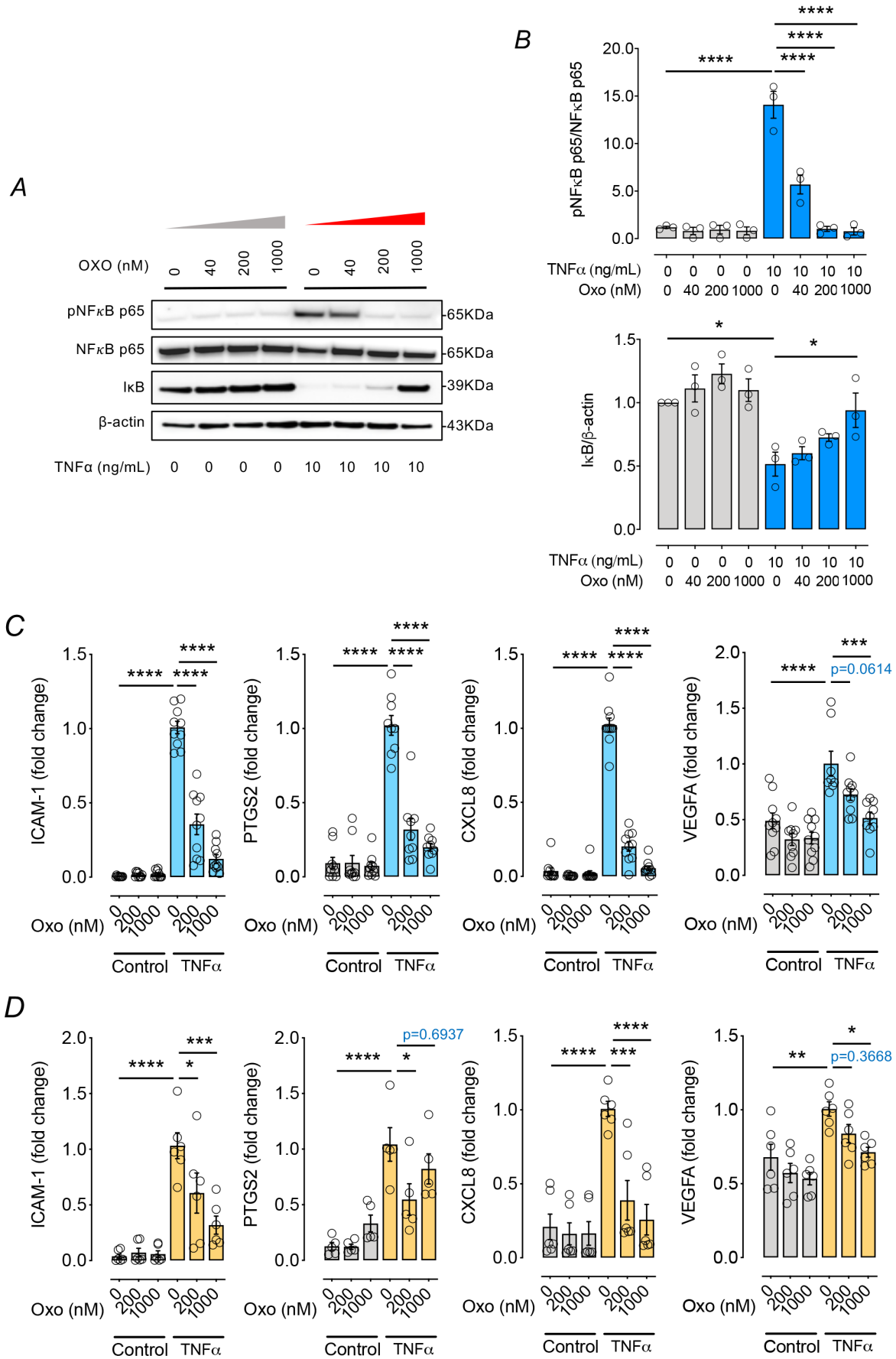
A
OXO (nM)
0 40 200 1000 0 40 200 1000
pNFκB p65
NFκB p65
IκB
β-actin
65KDa
65KDa
39KDa
43KDa
TNFα (ng/mL) 0 0 0 0 10 10 10 10
B
pNFκB p65/NFκB p65
TNFα (ng/mL) 0 0 0 0 10 10 10 10
Oxo (nM) 0 40 200 1000 0 40 200 1000
IκB/β-actin
C
ICAM-1 (fold change)
PTGS2 (fold change)
CXCL8 (fold change)
VEGFA (fold change)
p=0.0614
Oxo (nM)
Control
TNFα
D
p=0.6937
p=0.3668

648

649 **Fig. 4 Pharmacological inhibition of TAK1 by 5Z-7-oxozeaenol suppressed the NFκB pathway**
650 **and expression of related pro-inflammatory/pro-angiogenic genes in human endothelial cells.**
651 (A) TIME cells were pretreated with 5Z-7-oxozeaenol (Oxo) (40, 200 or 1000 nM) for 30 minutes,
652 followed by TNFα stimulation (10 ng/ml) for 10 minutes. Activation of NFκB signals was detected
653 using western blot (n = 3). (B) Western blot showed that pharmacological inhibition of TAK1 impairs
654 the activation of NFκB p65 and degradation of IκB in TIMEs. TIMEs (C) and HRMECs (D) were
655 pretreated with 5Z-7-oxozeaenol (oxo; 200 or 1000 nM) for 30 minutes, followed by exposure to TNFα
656 (10 ng/ml) for 24 hours to stimulate proinflammatory/pro-angiogenesis gene expression. qPCR
657 revealed that inhibition of TAK1 suppressed TNFα induced *ICAM-1*, *PTGS2* and *CXCL8* (but not
658 *VEGFA)* expressions in a dose-dependent manner (n = 3-5; technical duplicate from each biological
659 repeat was shown as separated dot plot). All data are shown as means ± SEM. Statistical analysis was
660 undertaken with one-way ANOVA and Tukey's multiple comparison test; *$P < 0.05$, **$P < 0.01$, ***P
661 < 0.001, ****$P < 0.0001$.
662
663

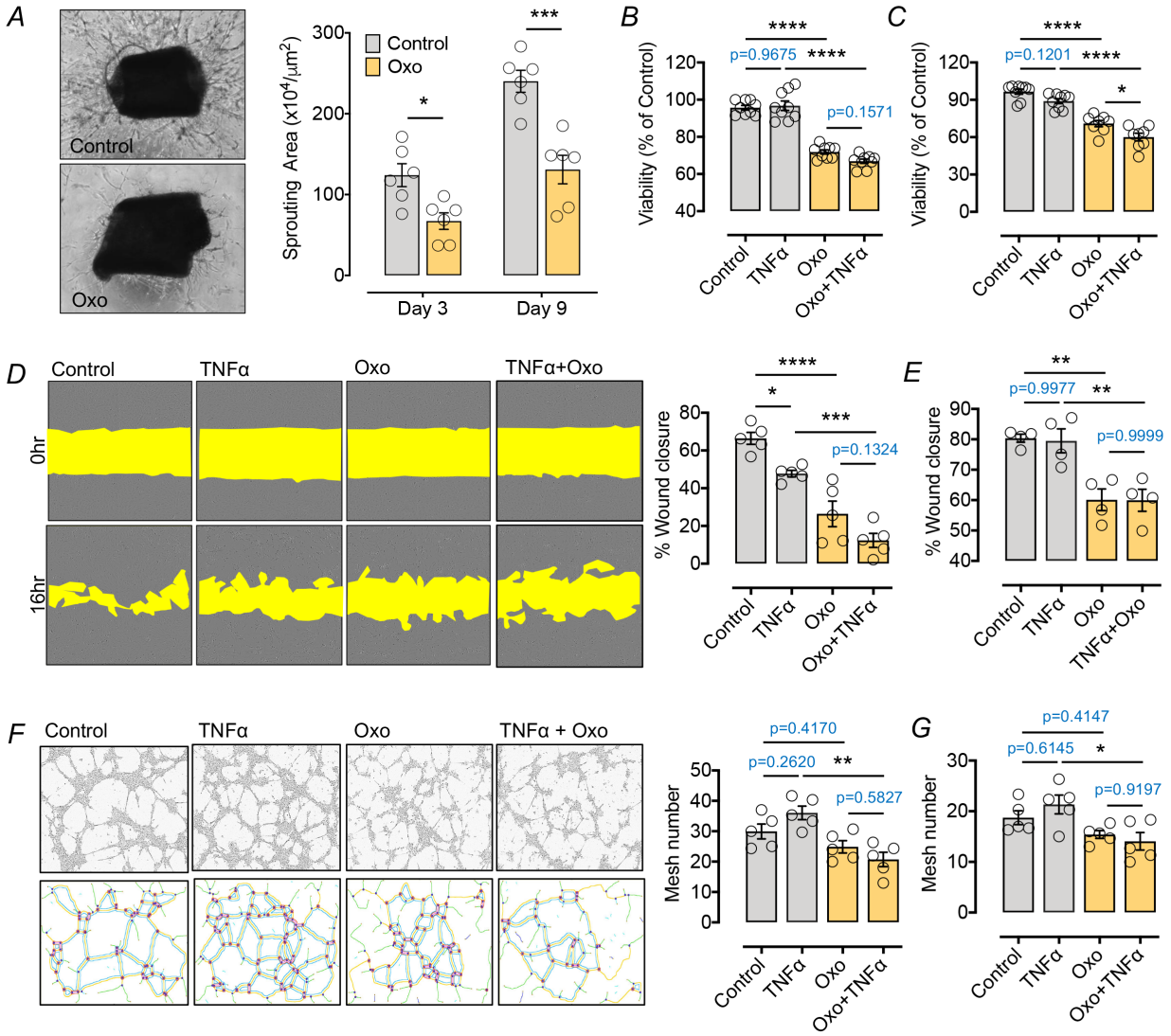

Fig. 5 TAK1 inhibition by 5Z-7-oxozeaenol attenuated angiogenesis in mouse tissues *ex vivo* and human endothelial cells *in vitro*.

(A) Endothelial cell sprouting assay performed in the presence or absence of the TAK1 inhibitor 5Z-7-oxozeaenol (Oxo) and the corresponding quantification of sprouting area at day 3 and day 9. Representative images were taken at day 9. Statistical analysis was undertaken with two-way ANOVA and Bonferroni's multiple comparisons test. (B-C) After pre-treatment with 5Z-7-oxozeaenol (oxo; 1 μM) in the presence or absence of TNFα (10 ng/ml) for 48 hours, MTT assay was performed to quantify cell viability. TAK1 inhibition by 5Z-7-oxozeaenol reduced cell viability in (B) TIMEs and (C) HRMECs (n = 3). Technical triplicate from each biological repeat was shown as separated dot plot. (D) After exposure to 5Z-7-oxozeaenol (1 μM) with or without TNFα (10 ng/ml), a wound healing assay was performed to evaluate migration activity in TIMEs. Representative images were taken after wounding (or scraping cells, 0 hr) and at 16 hours (16 hr) post-wounding. Quantitative analysis of cell

677 migration assay was characterized by wound closure (n = 5). (E) With same pre-treatment as Fig. 5D,
678 migration assay was performed in HRMECs (n = 4). (F) After exposing to 5Z-7-oxozeaenol (1 μM)
679 with or without TNFα (10 ng/ml) for 24 hours, tube formation assay was performed (n = 5).
680 Representative images were taken 6 hours post tube formation. Quantitative analysis was characterized
681 by mesh number. (G) With same pre-treatment as Fig. 5F, tube formation assay was performed in
682 HRMECs (n = 5). Group data are shown as means ± SEM. Statistical analysis was undertaken with
683 one-way ANOVA and Tukey's multiple comparison test; *$P < 0.05$, **$P < 0.01$, ***$P < 0.001$, ****P
684 < 0.0001.
685
686

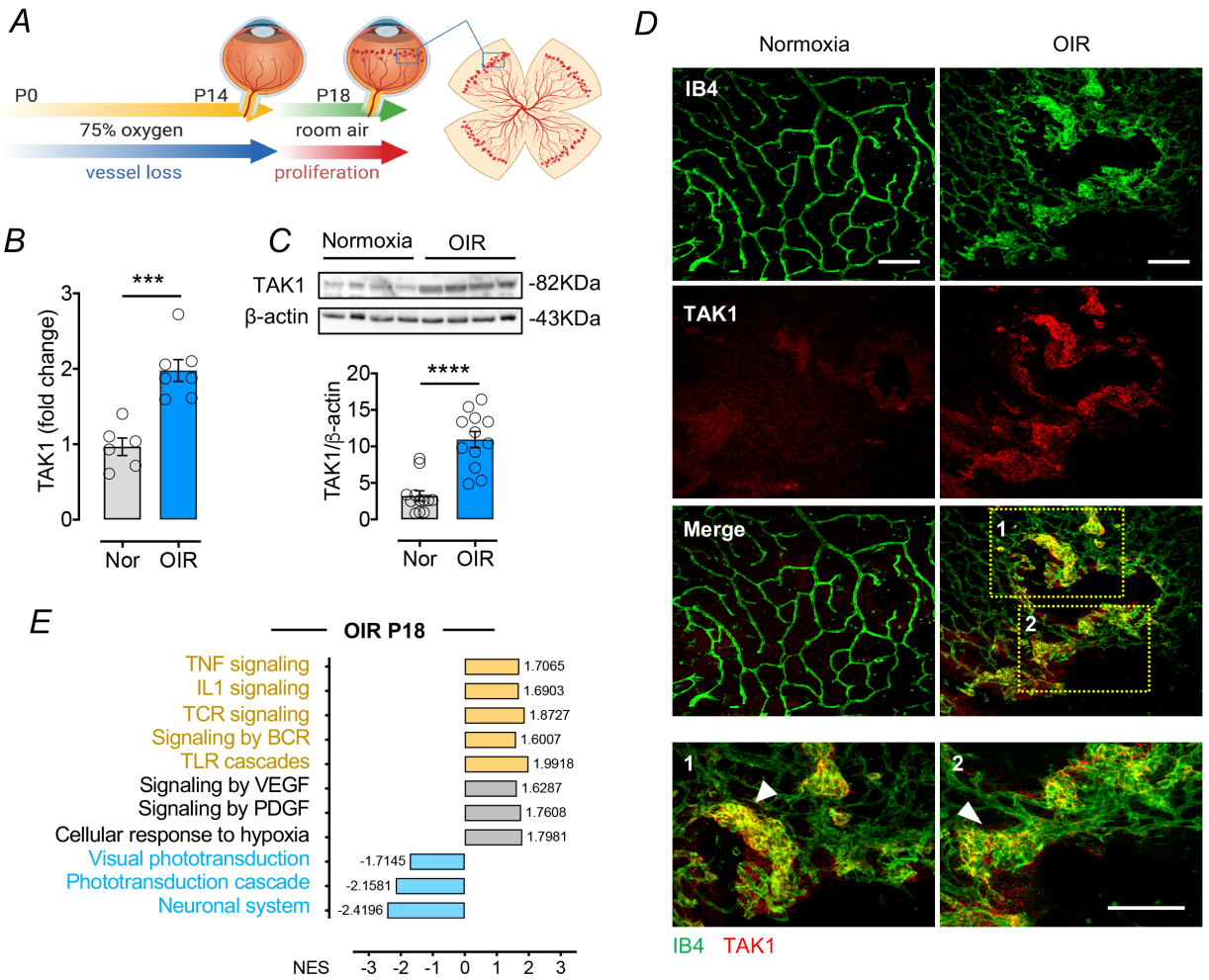

Fig. 6 Involvement of TAK1 in pathological retinal angiogenesis in a rat model of retinopathy. (A) Schematic diagram of the Sprague-Dawley rat model of oxygen-induced retinopathy (OIR). Neonatal rats were exposed to 80% of oxygen for 21 hours each day from postnatal day 0 (P0) to P14. Rats were returned to room air from P14 to P18. Vessel loss was induced during oxygen exposure and retinal angiogenesis could be induced after rats returned to room air. (B) qPCR analysis of *TAK1* expression in OIR at P18 as compared with the normoxia group (n = 6-7). (C) Western blot analysis of TAK1 expression in OIR at P18 compared with normoxia group (n = 10-12). Representative immunoblotting from 4 independent samples were shown for normoxia (lanes 1-4) and OIR group (lanes 5-8). (D) Immunobiological staining indicated expression of TAK1 in the pathological vessel. Vasculature were visualized by IB4 labelling (green) and counterstained with TAK1 (red) in retinal whole mount. Scale bar: 100 μm. (E) GSEA indicated that most of TAK1 upstream pathways including TNF, IL1, TCR, BCR, TLR, and VEGF pathways (from Reactome Pathway Database) were positively enriched in OIR at P18. Group data are shown as means ± SEM. Statistical analysis was undertaken with two-tailed unpaired t-test; ***$P < 0.001$, ****$P < 0.0001$.

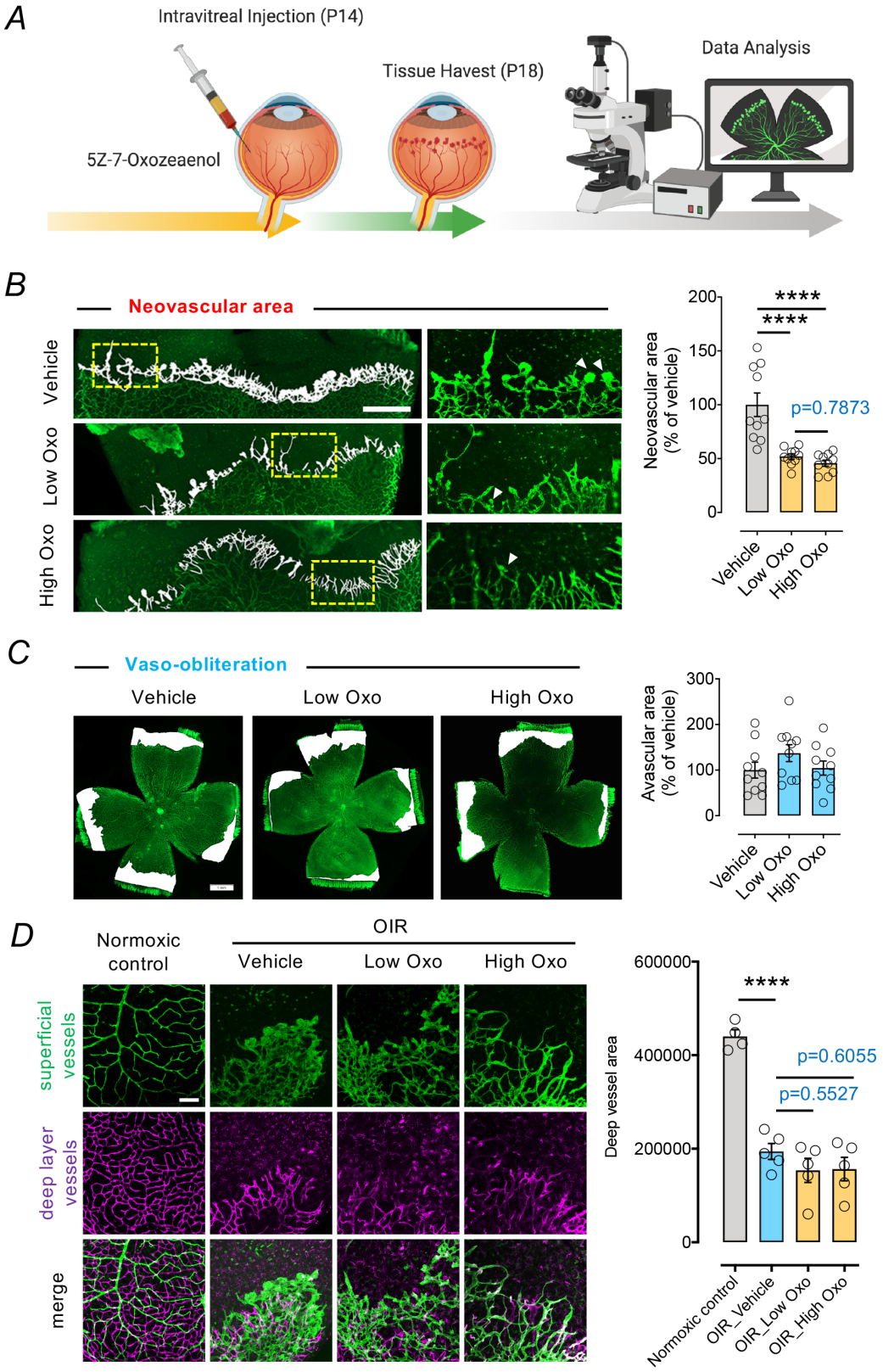

Fig. 7 TAK1 Inhibition by 5Z-7-oxozeaenol suppressed retinal angiogenesis in OIR rats.

704 (A) Experimental protocol for 5Z-7-oxozeaenol treatment in the OIR rat model. A single intravitreal
705 injection of vehicle, low (18 ng) or high (90 ng) dose of 5Z-7-oxozeaenol was given to Sprague-
706 Dawley OIR rats at P14, followed by quantitative analysis of retinal neovascularization of flat mounted
707 retinae at P18. (B) Retinal neovascularization is highlighted in white, and insets show selected areas
708 at high magnification. Arrowheads indicated vessel tufts. Retinal neovascularization was quantified
709 from 10 individual retinas per group. Scale bar: 500 μm. (C) Vaso-obliteration was simultaneously
710 evaluated with the same samples analyzed in Fig. 7B. The white areas represent the avascular area in
711 the retina. No significant difference was observed between groups (n = 10). Scale bar: 1 mm. (D)
712 Vessel area of superficial and deep vascular layers was quantified in P18 control (n = 4) and OIR rats
713 following a single intravitreal injection of vehicle, low or high dose of 5Z-7-oxozeaenol at P14 (n = 5
714 each group). Scale bar: 100 μm. Group data are shown as means ± SEM. Statistical analysis was
715 undertaken with one-way ANOVA and Tukey's multiple comparison test; ****$P < 0.0001$.
716
717

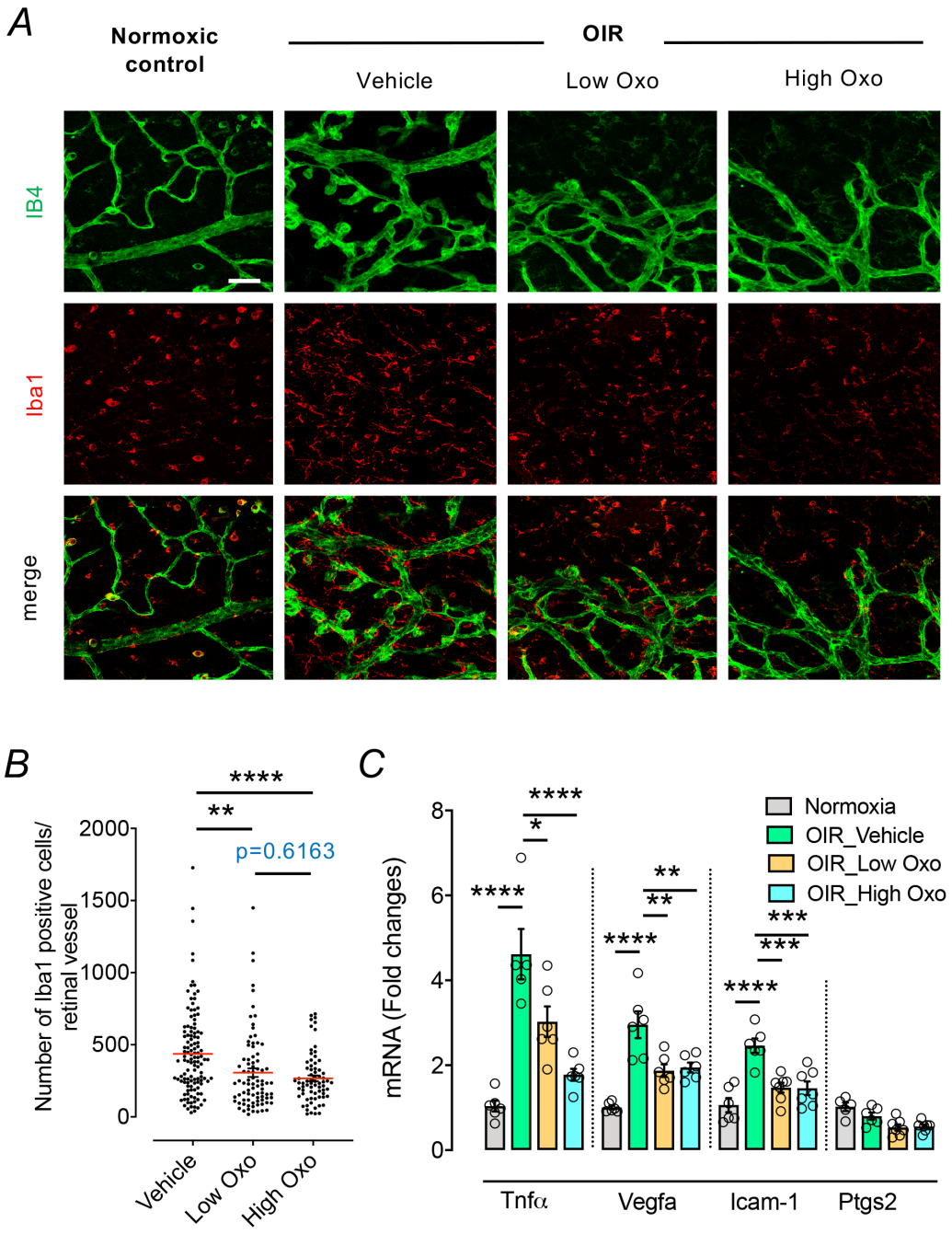

Fig. 8 TAK1 inhibition by 5Z-7-oxozeaenol inhibited the adhesion of microglia to vessels and inflammatory gene expression in OIR.

(A) Representative images of microglial adhesion to the vascular surface in a retina from a P18 control rat and P18 OIR rats that had a single intravitreal injection of vehicle, low or high dose of 5Z-7-oxozeaenol (Oxo) at P14. Vessels were visualized with IB4 staining (green), and distribution of microglia was immunolabeled with Iba-1 (red). Scale bar: 50 µm. (B) Quantitative analysis of microglial number relative to retinal vessel area in vehicle or 5Z-7-oxozeaenol treated OIR rats at

726 P18. (C) Intravitreal injection of 5Z-7-oxozeaenol in OIR rats at P14 inhibited proinflammatory (*TNFα*
727 and *ICAM-1*) and pro-angiogenesis (*VEGFA*) gene expression at P16 (n = 5-7). Group data are shown
728 as means ± SEM. Statistical analysis was undertaken with one-way ANOVA and Tukey's multiple
729 comparison test; *$P < 0.05$, **$P < 0.01$, ***$P < 0.001$, ****$P < 0.0001$.
730
731
732

733 **REFERENCES**

734 1. K. A. Neely, T. W. Gardner, Ocular neovascularization: clarifying complex interactions. *Am J*
735 *Pathol* **153**, 665-670 (1998).
736 2. P. A. Campochiaro, Retinal and choroidal neovascularization. *Journal of cellular physiology*
737 **184**, 301-310 (2000).
738 3. M. A. Singer, D. S. Kermany, J. Waters, M. E. Jansen, L. Tyler, Diabetic macular edema: it is
739 more than just VEGF. *F1000Res* **5**, (2016).
740 4. Y. Qazi, S. Maddula, B. K. Ambati, Mediators of ocular angiogenesis. *J Genet* **88**, 495-515
741 (2009).
742 5. R. B. Goldberg, Cytokine and cytokine-like inflammation markers, endothelial dysfunction,
743 and imbalanced coagulation in development of diabetes and its complications. *J Clin*
744 *Endocrinol Metab* **94**, 3171-3182 (2009).
745 6. N. Demircan, B. G. Safran, M. Soylu, A. A. Ozcan, S. Sizmaz, Determination of vitreous
746 interleukin-1 (IL-1) and tumour necrosis factor (TNF) levels in proliferative diabetic
747 retinopathy. *Eye (Lond)* **20**, 1366-1369 (2006).
748 7. M. Capitao, R. Soares, Angiogenesis and Inflammation Crosstalk in Diabetic Retinopathy. *J*
749 *Cell Biochem* **117**, 2443-2453 (2016).
750 8. P. Murugeswari, D. Shukla, A. Rajendran, R. Kim, P. Namperumalsamy, V. Muthukkaruppan,
751 Proinflammatory cytokines and angiogenic and anti-angiogenic factors in vitreous of patients
752 with proliferative diabetic retinopathy and eales' disease. *Retina* **28**, 817-824 (2008).
753 9. W. Stevenson, S. F. Cheng, M. H. Dastjerdi, G. Ferrari, R. Dana, Corneal neovascularization
754 and the utility of topical VEGF inhibition: ranibizumab (Lucentis) vs bevacizumab (Avastin).
755 *Ocul Surf* **10**, 67-83 (2012).
756 10. C. A. Aveleira, C. M. Lin, S. F. Abcouwer, A. F. Ambrosio, D. A. Antonetti, TNF-alpha signals
757 through PKCzeta/NF-kappaB to alter the tight junction complex and increase retinal
758 endothelial cell permeability. *Diabetes* **59**, 2872-2882 (2010).
759 11. M. Clauss, C. Sunderkotter, B. Sveinbjornsson, S. Hippenstiel, A. Willuweit, M. Marino, E.
760 Haas, R. Seljelid, P. Scheurich, N. Suttorp, M. Grell, W. Risau, A permissive role for tumor
761 necrosis factor in vascular endothelial growth factor-induced vascular permeability. *Blood* **97**,
762 1321-1329 (2001).
763 12. S. Yoshida, A. Yoshida, T. Ishibashi, Induction of IL-8, MCP-1, and bFGF by TNF-alpha in
764 retinal glial cells: implications for retinal neovascularization during post-ischemic
765 inflammation. *Graefes Arch Clin Exp Ophthalmol* **242**, 409-413 (2004).
766 13. A. M. Joussen, V. Poulaki, N. Mitsiades, B. Kirchhof, K. Koizumi, S. Dohmen, A. P. Adamis,
767 Nonsteroidal anti-inflammatory drugs prevent early diabetic retinopathy via TNF-alpha
768 suppression. *FASEB journal : official publication of the Federation of American Societies for*
769 *Experimental Biology* **16**, 438-440 (2002).
770 14. S. Sato, H. Sanjo, K. Takeda, J. Ninomiya-Tsuji, M. Yamamoto, T. Kawai, K. Matsumoto, O.

771 Takeuchi, S. Akira, Essential function for the kinase TAK1 in innate and adaptive immune
772 responses. *Nat Immunol* **6**, 1087-1095 (2005).
773 15. J. H. Shim, C. Xiao, A. E. Paschal, S. T. Bailey, P. Rao, M. S. Hayden, K. Y. Lee, C. Bussey,
774 M. Steckel, N. Tanaka, G. Yamada, S. Akira, K. Matsumoto, S. Ghosh, TAK1, but not TAB1
775 or TAB2, plays an essential role in multiple signaling pathways in vivo. *Genes Dev* **19**, 2668-
776 2681 (2005).
777 16. S. R. Mihaly, J. Ninomiya-Tsuji, S. Morioka, TAK1 control of cell death. *Cell death and*
778 *differentiation* **21**, 1667-1676 (2014).
779 17. S. A. Scarneo, A. Mansourati, L. S. Eibschutz, J. Totzke, J. R. Roques, D. Loiselle, D. Carlson,
780 P. Hughes, T. A. J. Haystead, Genetic and pharmacological validation of TAK1 inhibition in
781 macrophages as a therapeutic strategy to effectively inhibit TNF secretion. *Sci Rep* **8**, 17058
782 (2018).
783 18. K. B. Harikumar, B. Sung, S. T. Tharakan, M. K. Pandey, B. Joy, S. Guha, S. Krishnan, B. B.
784 Aggarwal, Sesamin manifests chemopreventive effects through the suppression of NF-kappa
785 B-regulated cell survival, proliferation, invasion, and angiogenic gene products. *Mol Cancer*
786 *Res* **8**, 751-761 (2010).
787 19. H. Naito, T. Iba, T. Wakabayashi, I. Tai-Nagara, J. I. Suehiro, W. Jia, D. Eino, S. Sakimoto, F.
788 Muramatsu, H. Kidoya, H. Sakurai, T. Satoh, S. Akira, Y. Kubota, N. Takakura, TAK1 Prevents
789 Endothelial Apoptosis and Maintains Vascular Integrity. *Dev Cell* **48**, 151-166 e157 (2019).
790 20. S. Morioka, M. Inagaki, Y. Komatsu, Y. Mishina, K. Matsumoto, J. Ninomiya-Tsuji, TAK1
791 kinase signaling regulates embryonic angiogenesis by modulating endothelial cell survival and
792 migration. *Blood* **120**, 3846-3857 (2012).
793 21. J. Schoneberg, F. De Lorenzi, B. Theek, A. Blaeser, D. Rommel, A. J. C. Kuehne, F. Kiessling,
794 H. Fischer, Engineering biofunctional in vitro vessel models using a multilayer bioprinting
795 technique. *Sci Rep* **8**, 10430 (2018).
796 22. A. Subramanian, P. Tamayo, V. K. Mootha, S. Mukherjee, B. L. Ebert, M. A. Gillette, A.
797 Paulovich, S. L. Pomeroy, T. R. Golub, E. S. Lander, J. P. Mesirov, Gene set enrichment
798 analysis: a knowledge-based approach for interpreting genome-wide expression profiles. *Proc*
799 *Natl Acad Sci U S A* **102**, 15545-15550 (2005).
800 23. S. Fechtner, D. A. Fox, S. Ahmed, Transforming growth factor beta activated kinase 1: a
801 potential therapeutic target for rheumatic diseases. *Rheumatology (Oxford)* **56**, 1060-1068
802 (2017).
803 24. S. Ghosh, M. Karin, Missing pieces in the NF-kappaB puzzle. *Cell* **109 Suppl**, S81-96 (2002).
804 25. T. Liu, L. Zhang, D. Joo, S. C. Sun, NF-kappaB signaling in inflammation. *Signal Transduct*
805 *Target Ther* **2**, (2017).
806 26. Y. Yang, Wu, J, and Wang, J.K., A database and functional annotation of NF-κB target genes.
807 *Int J Clin Exp Med* **9**, 7986-7995 (2016).
808 27. J. Ninomiya-Tsuji, T. Kajino, K. Ono, T. Ohtomo, M. Matsumoto, M. Shiina, M. Mihara, M.

809 Tsuchiya, K. Matsumoto, A resorcylic acid lactone, 5Z-7-oxozeaenol, prevents inflammation
810 by inhibiting the catalytic activity of TAK1 MAPK kinase kinase. *J Biol Chem* **278**, 18485-
811 18490 (2003).
812 28. S. F. Hackett, S. Wiegand, G. Yancopoulos, P. A. Campochiaro, Angiopoietin-2 plays an
813 important role in retinal angiogenesis. *J Cell Physiol* **192**, 182-187 (2002).
814 29. F. S. Sorrentino, M. Allkabes, G. Salsini, C. Bonifazzi, P. Perri, The importance of glial cells
815 in the homeostasis of the retinal microenvironment and their pivotal role in the course of
816 diabetic retinopathy. *Life Sci* **162**, 54-59 (2016).
817 30. J. Li, C. Liang, Z. K. Zhang, X. Pan, S. Peng, W. S. Lee, A. Lu, Z. Lin, G. Zhang, W. N. Leung,
818 B. T. Zhang, TAK1 inhibition attenuates both inflammation and fibrosis in experimental
819 pneumoconiosis. *Cell Discov* **3**, 17023 (2017).
820 31. L. Yang, S. Joseph, T. Sun, J. Hoffmann, S. Thevissen, S. Offermanns, B. Strilic, TAK1
821 regulates endothelial cell necroptosis and tumor metastasis. *Cell death and differentiation* **26**,
822 1987-1997 (2019).
823 32. L. Dai, C. Aye Thu, X. Y. Liu, J. Xi, P. C. Cheung, TAK1, more than just innate immunity.
824 *IUBMB Life* **64**, 825-834 (2012).
825 33. Y. Onodera, T. Teramura, T. Takehara, K. Shigi, K. Fukuda, Reactive oxygen species induce
826 Cox-2 expression via TAK1 activation in synovial fibroblast cells. *FEBS Open Bio* **5**, 492-501
827 (2015).
828 34. M. Xie, D. Zhang, J. R. Dyck, Y. Li, H. Zhang, M. Morishima, D. L. Mann, G. E. Taffet, A.
829 Baldini, D. S. Khoury, M. D. Schneider, A pivotal role for endogenous TGF-beta-activated
830 kinase-1 in the LKB1/AMP-activated protein kinase energy-sensor pathway. *Proc Natl Acad*
831 *Sci U S A* **103**, 17378-17383 (2006).
832 35. H. Sakurai, Targeting of TAK1 in inflammatory disorders and cancer. *Trends in*
833 *pharmacological sciences* **33**, 522-530 (2012).
834 36. G. Sabio, R. J. Davis, TNF and MAP kinase signalling pathways. *Semin Immunol* **26**, 237-245
835 (2014).
836 37. J. Landry, J. Huot, Regulation of actin dynamics by stress-activated protein kinase 2 (SAPK2)-
837 dependent phosphorylation of heat-shock protein of 27 kDa (Hsp27). *Biochem Soc Symp* **64**,
838 79-89 (1999).
839 38. R. Munoz-Chapuli, A. R. Quesada, M. Angel Medina, Angiogenesis and signal transduction in
840 endothelial cells. *Cell Mol Life Sci* **61**, 2224-2243 (2004).
841 39. M. Tang, X. Wei, Y. Guo, P. Breslin, S. Zhang, S. Zhang, W. Wei, Z. Xia, M. Diaz, S. Akira, J.
842 Zhang, TAK1 is required for the survival of hematopoietic cells and hepatocytes in mice. *The*
843 *Journal of experimental medicine* **205**, 1611-1619 (2008).
844 40. K. Schulze-Osthoff, D. Ferrari, K. Riehemann, S. Wesselborg, Regulation of NF-kappa B
845 activation by MAP kinase cascades. *Immunobiology* **198**, 35-49 (1997).
846 41. J. Wu, F. Powell, N. A. Larsen, Z. Lai, K. F. Byth, J. Read, R. F. Gu, M. Roth, D. Toader, J. C.

847 Saeh, H. Chen, Mechanism and in vitro pharmacology of TAK1 inhibition by (5Z)-7-
848 Oxozeaenol. *ACS chemical biology* **8**, 643-650 (2013).
849 42. J. J. Cohen, Apoptosis. *Immunol Today* **14**, 126-130 (1993).
850 43. D. Zhang, H. Yan, H. Li, S. Hao, Z. Zhuang, M. Liu, Q. Sun, Y. Yang, M. Zhou, K. Li, C. Hang,
851 TGFbeta-activated Kinase 1 (TAK1) Inhibition by 5Z-7-Oxozeaenol Attenuates Early Brain
852 Injury after Experimental Subarachnoid Hemorrhage. *The Journal of biological chemistry* **290**,
853 19900-19909 (2015).
854 44. L. Lu, X. Zhang, H. Tong, W. Zhang, P. Xu, S. Qu, Central Administration of 5Z-7-Oxozeaenol
855 Protects Experimental Autoimmune Encephalomyelitis Mice by Inhibiting Microglia
856 Activation. *Front Pharmacol* **8**, 789 (2017).
857 45. T. D. Merson, M. D. Binder, T. J. Kilpatrick, Role of cytokines as mediators and regulators of
858 microglial activity in inflammatory demyelination of the CNS. *Neuromolecular Med* **12**, 99-
859 132 (2010).
860 46. B. J. White, S. Tarabishy, V. R. Venna, B. Manwani, S. Benashski, L. D. McCullough, J. Li,
861 Protection from cerebral ischemia by inhibition of TGFbeta-activated kinase. *Exp Neurol* **237**,
862 238-245 (2012).
863 47. M. Ivshina, I. M. Alexandrov, A. Vertii, S. Doxsey, J. D. Richter, CPEB regulation of TAK1
864 synthesis mediates cytokine production and the inflammatory immune response. *Mol Cell Biol*
865 **35**, 610-618 (2015).
866 48. D. J. Ireland, M. W. Kemp, Y. Miura, M. Saito, J. P. Newnham, J. A. Keelan, Intra-amniotic
867 pharmacological blockade of inflammatory signalling pathways in an ovine chorioamnionitis
868 model. *Mol Hum Reprod* **21**, 479-489 (2015).
869 49. M. Neubert, D. A. Ridder, P. Bargiotas, S. Akira, M. Schwaninger, Acute inhibition of TAK1
870 protects against neuronal death in cerebral ischemia. *Cell death and differentiation* **18**, 1521-
871 1530 (2011).
872 50. K. Bettermann, M. Vucur, J. Haybaeck, C. Koppe, J. Janssen, F. Heymann, A. Weber, R.
873 Weiskirchen, C. Liedtke, N. Gassler, M. Muller, R. de Vos, M. J. Wolf, Y. Boege, G. M.
874 Seleznik, N. Zeller, D. Erny, T. Fuchs, S. Zoller, S. Cairo, M. A. Buendia, M. Prinz, S. Akira,
875 F. Tacke, M. Heikenwalder, C. Trautwein, T. Luedde, TAK1 suppresses a NEMO-dependent
876 but NF-kappaB-independent pathway to liver cancer. *Cancer Cell* **17**, 481-496 (2010).
877 51. E. Omori, S. Morioka, K. Matsumoto, J. Ninomiya-Tsuji, TAK1 regulates reactive oxygen
878 species and cell death in keratinocytes, which is essential for skin integrity. *J Biol Chem* **283**,
879 26161-26168 (2008).
880 52. B. V. Bui, B. Fortune, Ganglion cell contributions to the rat full-field electroretinogram. *J*
881 *Physiol* **555**, 153-173 (2004).
882 53. H. Cao, J. Lu, J. Du, F. Xia, S. Wei, X. Liu, T. Liu, Y. Liu, M. Xiang, TAK1 inhibition prevents
883 the development of autoimmune diabetes in NOD mice. *Sci Rep* **5**, 14593 (2015).
884 54. L. Tan, D. Gurbani, E. L. Weisberg, D. S. Jones, S. Rao, W. D. Singer, F. M. Bernard, S. Mowafy,

A. Jenney, G. Du, A. Nonami, J. D. Griffin, D. A. Lauffenburger, K. D. Westover, P. K. Sorger, N. S. Gray, Studies of TAK1-centered polypharmacology with novel covalent TAK1 inhibitors. *Bioorg Med Chem* **25**, 1320-1328 (2017).

55. A. Butler, P. Hoffman, P. Smibert, E. Papalexi, R. Satija, Integrating single-cell transcriptomic data across different conditions, technologies, and species. *Nat Biotechnol* **36**, 411-420 (2018).

56. T. Stuart, A. Butler, P. Hoffman, C. Hafemeister, E. Papalexi, W. M. Mauck, 3rd, Y. Hao, M. Stoeckius, P. Smibert, R. Satija, Comprehensive Integration of Single-Cell Data. *Cell* **177**, 1888-1902 e1821 (2019).

57. M. Baker, S. D. Robinson, T. Lechertier, P. R. Barber, B. Tavora, G. D'Amico, D. T. Jones, B. Vojnovic, K. Hodivala-Dilke, Use of the mouse aortic ring assay to study angiogenesis. *Nature protocols* **7**, 89-104 (2012).

58. D. Donovan, N. J. Brown, E. T. Bishop, C. E. Lewis, Comparison of three in vitro human 'angiogenesis' assays with capillaries formed in vivo. *Angiogenesis* **4**, 113-121 (2001).

59. J. S. Penn, B. L. Tolman, M. M. Henry, Oxygen-induced retinopathy in the rat: relationship of retinal nonperfusion to subsequent neovascularization. *Invest Ophthalmol Vis Sci* **35**, 3429-3435 (1994).

60. Y. S. Bee, L. Tu, S. J. Sheu, H. C. Lin, J. H. Tang, J. H. Wang, S. M. Prea, G. J. Dusting, D. C. Wu, J. Zhong, B. V. Bui, M. H. Tai, G. S. Liu, Gene Delivery of Calreticulin Anti-Angiogenic Domain Attenuates the Development of Choroidal Neovascularization in Rats. *Hum Gene Ther* **28**, 403-414 (2017).

61. K. M. Connor, N. M. Krah, R. J. Dennison, C. M. Aderman, J. Chen, K. I. Guerin, P. Sapieha, A. Stahl, K. L. Willett, L. E. H. Smith, Quantification of oxygen-induced retinopathy in the mouse: a model of vessel loss, vessel regrowth and pathological angiogenesis. *Nat Protoc* **4**, 1565-1573 (2009).

62. E. Zudaire, L. Gambardella, C. Kurcz, S. Vermeren, A computational tool for quantitative analysis of vascular networks. *PLoS One* **6**, e27385 (2011).

63. D. Zhao, C. T. Nguyen, V. H. Wong, J. K. Lim, Z. He, A. I. Jobling, E. L. Fletcher, H. R. Chinnery, A. J. Vingrys, B. V. Bui, Characterization of the Circumlimbal Suture Model of Chronic IOP Elevation in Mice and Assessment of Changes in Gene Expression of Stretch Sensitive Channels. *Front Neurosci* **11**, 41 (2017).

916 **SUPPLEMENTARY MATERIALS**

917 **SUPPLEMENTARY TABLE**

918 **Table S1. Key Resources table**

REAGENT or RESOURCE	SOURCE	IDENTIFIER
Antibodies		
IκBα (L35A5) mouse mAb	Cell Signaling Technology	4814
Phospho-NFκB p65 (Ser536) (93H1) rabbit mAb	Cell Signaling Technology	3033
NFκB p65 (C22B4) rabbit mAb	Cell Signaling Technology	4764
Phospho-p44/42 MAPK (Erk1/2) (Thr202/Tyr204) rabbit pAb	Cell Signaling Technology	9101
p44/42 MAPK (Erk1/2) (137F5) rabbit mAb	Cell Signaling Technology	4695
Phospho-TAK1 (Ser412) rabbit pAb	Cell Signaling Technology	9339
TAK1 rabbit pAb	Cell Signaling Technology	4505
Phospho-SAPK/JNK (Thr183/Tyr185) (G9) mouse mAb	Cell Signaling Technology	9255
SAPK/JNK rabbit pAb	Cell Signaling Technology	9252
Phospho-p38 MAPK (Thr180/Tyr182) rabbit pAb	Cell Signaling Technology	9211
p38 MAPK (D13E1) XP® rabbit mAb	Cell Signaling Technology	8690
Actin (clone C4) mouse mAb	Merck Millipore	MAB1501
TAK1 rabbit pAb	Novus Biologicals	NBP1-87819
Human CD31 mouse mAb	DAKO	M0823
Iba1 rabbit pAb	FUJIFILM Wako Chemicals	019-19741
Isolectin GS-IB4 from Griffonia simplicifolia, Alexa Fluor™ 488 conjugate	Life Technologies Australia	I21411
Goat anti-mouse IgG HRP-conjugated secondary Ab	Merck Millipore	12-349

Goat anti-rabbit Alexa Fluor 488 plus secondary Ab	Invitrogen	A32731
Goat anti-mouse Alexa Fluor 594 plus secondary Ab	Invitrogen	A32742
NucBlue™ Reagent (Hoechst 33342)	Life Technologies Australia	R37605
Chemicals		
5Z-7-oxozeaenol	Tocris Bioscience	3604/1
3-(4,5-dimethylthiazol-2-yl)-2,5-diphenyl-2H-tetrazolium bromide (MTT)	Sigma-Aldrich	M2128
DMSO	Sigma-Aldrich	D8418
Sodium citrate dihydrate	Sigma-Aldrich	W302600
Triton X100	Sigma-Aldrich	T8787
Ampicillin	Sigma-Aldrich	A0166
Polybrene	Sigma-Aldrich	H9268
Puromycin	Sigma-Aldrich	P8833
Agarose	Sigma-Aldrich	A6361
Critical Commercial Assays		
Pierce™ BCA assay kit	Life Technologies Australia	23227
Amersham ECL Prime Western Blotting Detection Kit	GE Healthcare	RPN2232
Q5 Hot Start High-Fidelity 2X Master Mix	New England Biolabs	M0494
High-capacity cDNA reverse transcription Kit	Life Technologies Australia	4368814
TaqMan™ Fast Advanced Master Mix	Life Technologies Australia	4444553
Quick-RNA MiniPrep kit	Zymo Research	R1055
Agencourt CleanSeq Kit	Beckman Coulter	A29151
ZymoPURE Plasmid Miniprep Kit	Zymo Research	D4210
Quick-DNA Microprep Kit	Zymo Research	D3021
Experimental Models: Cell Lines		
Telomerase-immortalized human microvascular endothelial cells (TIMEs)	American Type Culture Collection	ATCC® CRL-4025™
Human retinal microvascular endothelial cells (HRMECs)	Cell Systems	ACBRI 181 V

Human embryonic kidney 293A	Life Technologies Australia	R70507
Human Müller glia cells (MIO-M1)	Institute of Ophthalmology, UCL	n/a
Experimental Models: Organisms/Strains		
Sprague-Dawley rat and C57BL/6 mouse	St Vincent's Hospital	004/16
Brown Norway rat	University of Melbourne	13-044UM
Sprague-Dawley rat	University of Tasmania	A0017311
Oligonucleotides		
TAK1 sgRNA#1 Forward	Integrated DNA Technologies	CACCGTAGACCAACAACGAGTCATC
TAK1 sgRNA#1 Reverse	Integrated DNA Technologies	AAACGATGACTCGTTGTTGGTCTAC
TAK1 sgRNA#2 Forward	Integrated DNA Technologies	CACCGGAGTTGTTTGCAAAGCTAAG
TAK1 sgRNA#2 Reverse	Integrated DNA Technologies	AAACCTTAGCTTTGCAAACAACTCC
TAK1 sgRNA#3 Forward	Integrated DNA Technologies	CACCGGAGGAAAGCGTTTATTGTAG
TAK1 sgRNA#3 Reverse	Integrated DNA Technologies	AAACCTACAATAAACGCTTTCCTCC
TAK1 sgRNA cassettes PCR Forward	Integrated DNA Technologies	TGAGTATTACGGCATGTGAGGGC
TAK1 sgRNA cassettes PCR Reverse	Integrated DNA Technologies	TCAATGTATCTTATCATGTCTGCTCGA
Human MAP3K7 siRNA (Smartpool)	Dharmacon	n/a
Human Control siRNA	Dharmacon	n/a
qPCR Probes		
Rat Map3k7 TaqMan probe	Applied Biosystems	Rn01437015_m1
Rat Tnf alpha TaqMan probe	Applied Biosystems	Rn01525859_g1
Rat Vegf-a TaqMan probe	Applied Biosystems	Rn01511602_m1
Rat Icam-1 TaqMan probe	Applied Biosystems	Rn00564227
Rat Ptgs2 TaqMan probe	Applied Biosystems	Rn01483828_m1
Rat beta actin TaqMan probe	Applied Biosystems	Rn00821065_g1
Human MAP3K7 TaqMan probe	Applied Biosystems	Hs00177373_m1
Human VEGF-A TaqMan probe	Applied Biosystems	Hs00900055_m1

Human ICAM-1 TaqMan probe	Applied Biosystems	Hs00164932_m1
Human VCAM-1 TaqMan probe	Applied Biosystems	Hs01003372_m1
Human CXCL8 TaqMan probe	Applied Biosystems	Hs00174103_m1
Human PTGS2 TaqMan probe	Applied Biosystems	Hs00153133_m1
Human GAPDH TaqMan probe	Applied Biosystems	Hs99999905_m1
Software and Algorithms		
Image Pro Plus	Media Cybernetics	n/a
Incucyte® Live-Cell Imaging and Analysis System	Sartorius	n/a
ImageJ version 1.48	Schneider et al., 2012 https://imagej.nih.gov/ij	n/a
Adobe Photoshop	Adobe. Connor et al., 2009	n/a
AngioTool Software	NIH. Zudaire et al., 2011	n/a
FIJI software	https://fiji.sc/	n/a
Prism 7	GraphPad Software	n/a
R (v4.0.2)	Bioconductor	n/a
Trimgalore (0.4.4)	Babraham Institute	n/a
STAR (2.5.3)	Alexander Dobin	n/a
FeatureCounts (subread 1.6.4)	Liao Y, Smyth GK and Shi W., 2014	n/a
Other		
Pierce RIPA buffer	Life Technologies Australia	89900
Protease inhibitor cocktail	Roche Diagnostics	11697498001
Recombinant Human TNF-α protein	Gibco™	PHC3015
Bolt™ 4-12% Bis-Tris Plus Gel	Invitrogen	NW04120BOX
Immun-Blot® PVDF Membrane	Bio-Rad Laboratories	1620177
Human VEGF protein	R&D Systems	293-VE-010
Matrigel™ Basement Membrane Matrix	Corning	356234
Normal donkey serum	Sigma-Aldrich	D9663
PBS	Gibco™	14190-144
Antibody Diluent	DAKO	S0809
Fluorescence Mounting Medium	DAKO	S3023
BsmBI	New England Biolabs	R0580S

lentiCRISPRv2 plasmid	Addgene	52961
NEB Stable Competent E. coli cells	New England Biolabs	C3040I
pCMV-dR8.91 (plasmid)	RNAiCore; Academia Sinica, Taipei, Taiwan	n/a
pMD2.G (plamid)	Addgene	12259
Lipofectamine 2000	Life Technologies Australia	11668019
0.45µm PDVF syringe filter	Merck Millipore	SLHV033RS
5x PEG-it	System Biosciences	LV810A-1
Opti-MEM	Life Technologies Australia	31985070
EBMTM Plus Basal Medium supplied with EGMTM Plus SingleQuotsTM supplements	Lonza	CC-5035
MycoAlert™ Mycoplasma Detection Kit	Lonza	LT07
Dulbecco's modified Eagle's medium	Life Technologies Australia	11965092
Glutamine	Life Technologies Australia	2503008
Penicillin-streptomycin	Life Technologies Australia	15070063
Fetal bovine serum	Sigma-Aldrich	F9423
TrypLE Express Enzyme (1X)	Life Technologies Australia	12605028

919

920

921 **SUPPLEMENTARY METHODS**

922 **Generation of TAK1-KO TIME cell line**

923 Three sgRNAs targeting the exonic regions of the human TAK1 gene (**Table S1**) were designed on
924 CHOPCHOP (https://chopchop.cbu.uib.no). The annealed oligos ordered from the Integrated DNA
925 Technologies (IDT; Coralville, Iowa, USA) representing the various sgRNAs were cloned into the
926 BsmBI sites (R0580S; New England Biolabs) of the lentiCRISPRv2 plasmid (52961; Addgene). The
927 plasmid was validated by Sanger sequencing with 3500 Series Genetic Analyzers (Thermo Fisher
928 Scientific; Waltham, MA). HEK293FT cells (R70007; Life Technologies) were plated at 1×10^7 cells
929 per T75 flask one day prior to transfection. Lentivirus was made by co-transfecting lentiCRISPRv2
930 (15µg), pCMV Δ8.91 (15µg) and pMDG plasmids (1.5µg) (RNAiCore; Academia Sinica, Taipei,
931 Taiwan) in HEK293FT cells using Lipofectamine 2000 (11668019; Life Technologies). Media was
932 changed 5 hours post transfection. The virus-containing media was harvested and filtered through a
933 0.45 µm PDVF syringe filter (SLHV033RS; Merck Millipore) to remove cell debris 48 hours post
934 transfection. Lentivirus aliquots were precipitated by 5x PEG-it (LV810A-1; System Biosciences) at
935 4°C overnight and centrifugated at 1500g at 4°C for 30 minutes. After discarding the supernatant, the
936 lentivirus were resuspend within opti-MEM ready for use. Wild type TIME cells (7.5×10^5) were plated
937 at T75 flask before transduction. When grow to 50% confluence, cells were transduced by TAK1
938 sgRNA lentiCRISPRv2 lentivirus with polybrene (8µg/mL) (H9268; Sigma-Aldrich) for 72 hours.
939 Medium containing 0.5 µg/mL puromycin (P8833; Sigma-Aldrich) was then replaced for another 72
940 hours to select stable clones which were subsequently cultured as the stable TAK1 KO cell lines.

941

942 **Single colony selection of TAK1-KO cell line**

943 Once the selected TAK1 KO cell lines reached 80% confluence, cells were trypsinized from the stable
944 cell pool using TrypLE Express Enzyme (1X) (12605028; Life Technologies) to break up any clumps
945 into individual cells. TAK1-KO cells were then diluted to a density of 5 cells/mL and resuspended
946 with 100 ul placed in each well in 96-well plate. After expanding for 7-14 days, colonies of single cells
947 were subsequently cultured as the single colony selected TAK1-KO cell line in culture dishes by
948 trypsinization.

949

950 **Identification of TAK1 indels in TAK1-KO line**

951 Genomic DNA was isolated from wild type and TAK1-KO TIME cell lines using Quick-DNA
952 Microprep Kit (D3021; Zymo Research) according to the manual. Extracted genomic DNA was used
953 as a PCR template to amplify the target of the TAK1 sgRNA using sequence specific primers (**Table**
954 **S1**). Briefly, PCR reactions were made up to 25 µL comprising 12.5 µL Q5 Hot Start High-Fidelity

955 2X Master Mix (M0494; New England Biolabs), 1.25 µL of forward and reverse primers and the
956 diluted gDNA, under thermocycling conditions of 98°C initial denaturation for 30 seconds, and 30
957 cycles of 98°C denaturation for 10 seconds, 65°C annealing for 30 seconds, and 72°C extension for 30
958 seconds with a 72°C final extension for 2 minutes. The PCR amplification product was validated using
959 electrophoresis using 1% agarose gel (A6361; Sigma-Aldrich). The gDNA was then cleaned by using
960 a Quick-DNA Microprep Kit (D3021; Zymo Research). Following the first-round of PCR
961 amplification, a second round of sequencing PCR was performed. The second-round PCR products
962 were subsequently purified using Agencourt CleanSeq Kit (A29151; Beckman Coulter). The PCR
963 samples were denatured at 98°C for 5 minutes and sequenced by Sanger sequencing.
964
965 **Electroretinography (ERG) in rat**
966 Rats were dark-adapted overnight prior to the ERG assessment under fully dark-adapted conditions.
967 Details for functional assessment are as previously described (*63*). Briefly, a pair of custom-made
968 chloride silver active and ring-shaped reference electrodes (99.9%, A&E Metal Merchants, Sydney,
969 NSW, AU), connected to platinum leads (F-E-30, Grass Telefactor, West Warwick, RI), was place on
970 the central cornea and around the sclera, respectively. A stainless-steel needle electrode (F-E2-30,
971 Grass Telefactor) was inserted subcutaneously into the tail of the animal to act as the ground.
972 Measurements were recorded simultaneously for both eyes. ERG analysis was undertaken as
973 previously described to return measures for three major waveforms, which are known to reflects the
974 function of key retinal cells, specifically photoreceptors (a-wave), bipolar cells (b-wave), and ganglion
975 cells (scotopic threshold response, STR).
976
977 **Spectral-domain optical coherence tomography (OCT) in rat**
978 Following ERG measurement, rat eyes were imaged using Envisu R2200 VHR spectral domain-OCT
979 (Bioptigen, Inc., Morrisville, NC, USA). Volume scans consisting of 1000 A-scans per 100 B-scans
980 (100 horizontal B-scans evenly spaced in the 1.4 mm vertical dimension) centered on the optic nerve
981 head (ONH; 1.4 × 1.4 × 1.57 mm) were obtained from both eyes. Four B-scans that crossed the ONH
982 were analyzed using FIJI software (https://fiji.sc/). In each B-scan the inner limiting membrane, retinal
983 nerve fiber layer, inner plexiform layer and Bruch's membrane were manually segmented by a masked
984 observer as previously described (*63*). Total retinal thickness was measured from the inner limiting to
985 Bruch's membrane. Retinal nerve fiber layer thickness was measured from the inner limiting
986 membrane to the inner aspect of the inner plexiform layer. Outer retinal thickness was measured from
987 Bruch's membrane to the outer plexiform layer.

988 **SUPPLEMENTARY FIGURES**

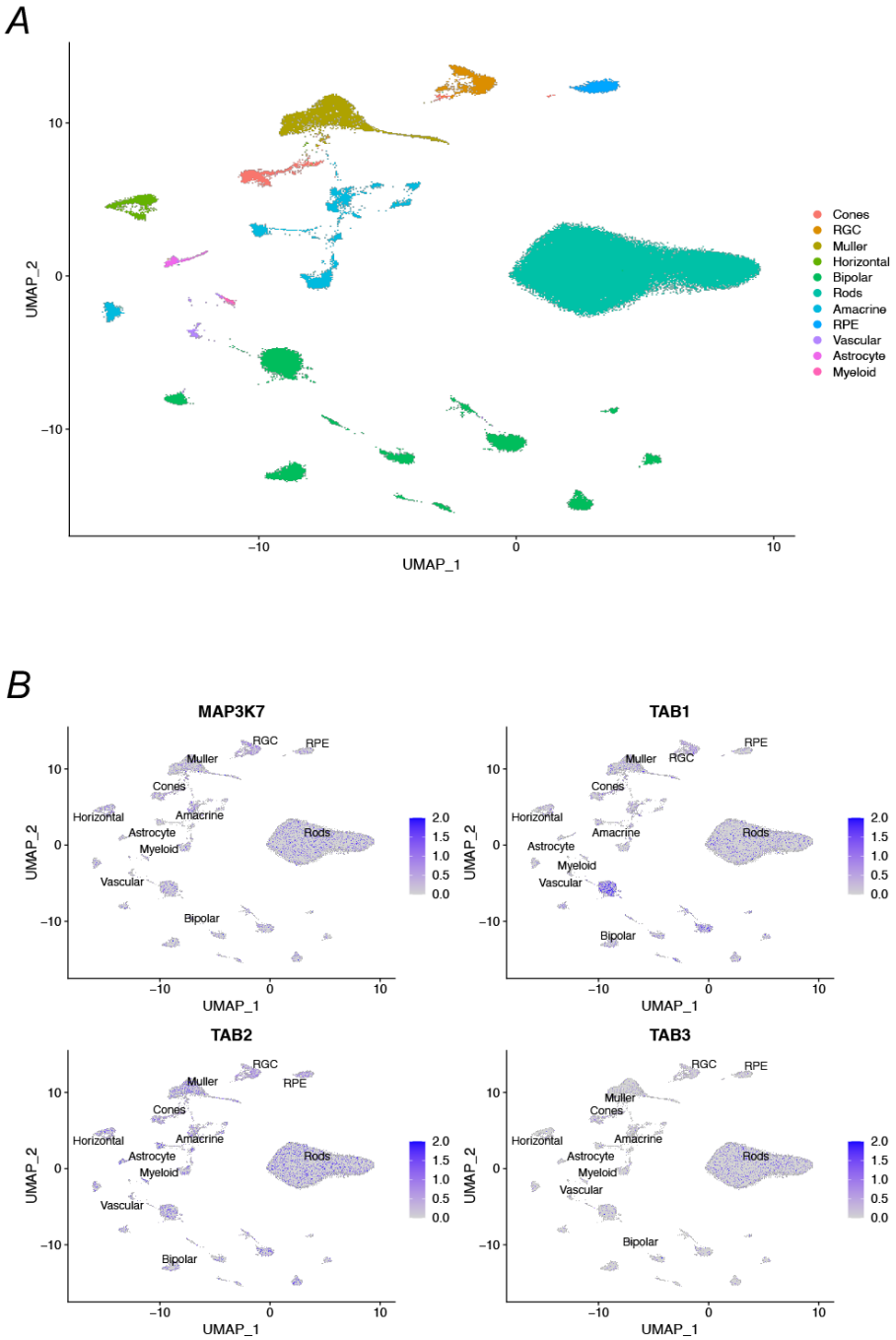

989

990 **Fig. S1** Uniform Manifold Approximation and Projection (UMAP) clustering of the integrated datasets
991 from snRNA-seq data (A) representing the expressions of TAK1 (MAP3K7) and TAK1-associated
992 proteins (TAB1-3) in identified retinal and non-retinal cellular clusters (B).

993

994

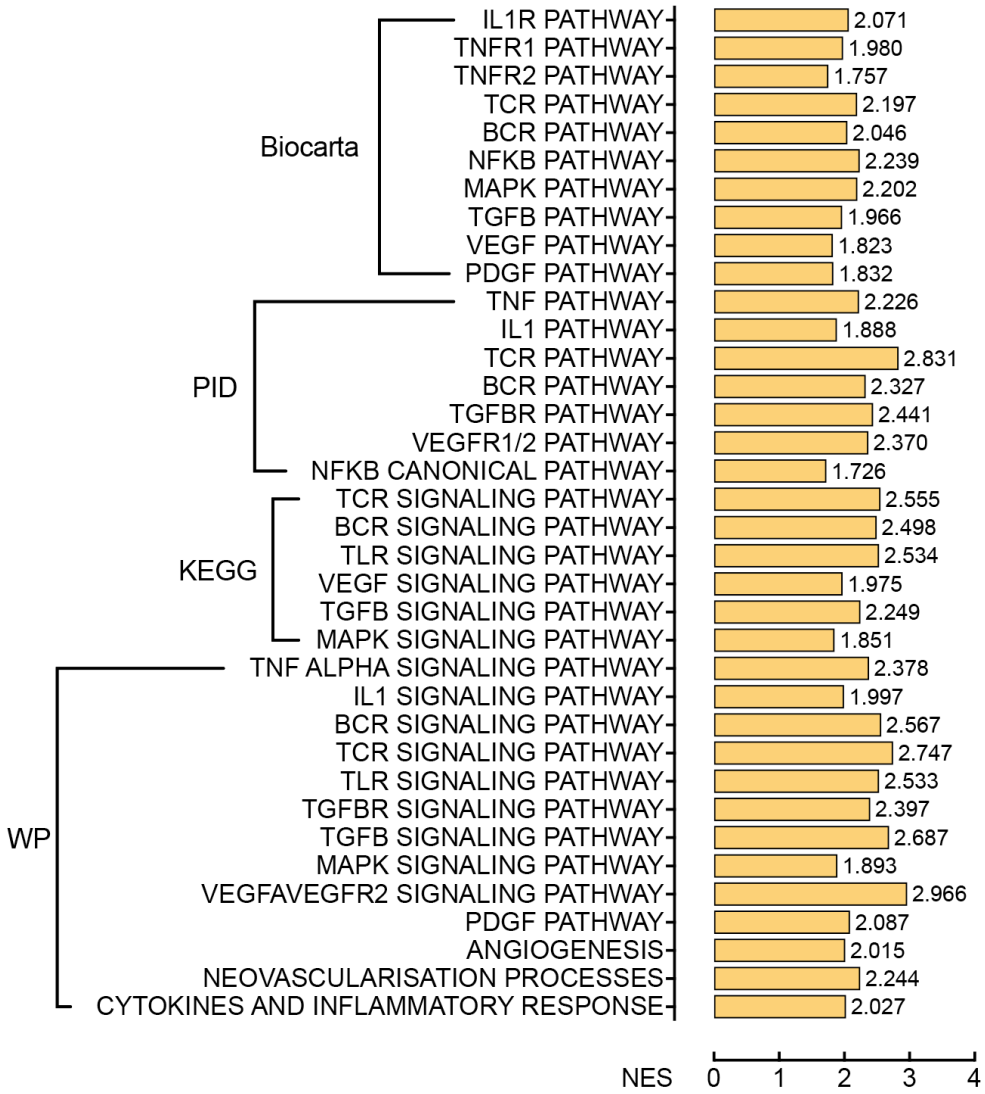

Fig. S2 Gene set enrichment analysis (GSEA) revealed positive enrichment of TAK1 upstream pathways in retinae from patients with retinal neovascularization due to proliferative diabetic retinopathy. Gene set database includes Biocarta, Pathway Interaction Database (PID), Kyoto Encyclopedia of Genes and Genomes (KEGG) and WikiPathways (WP).

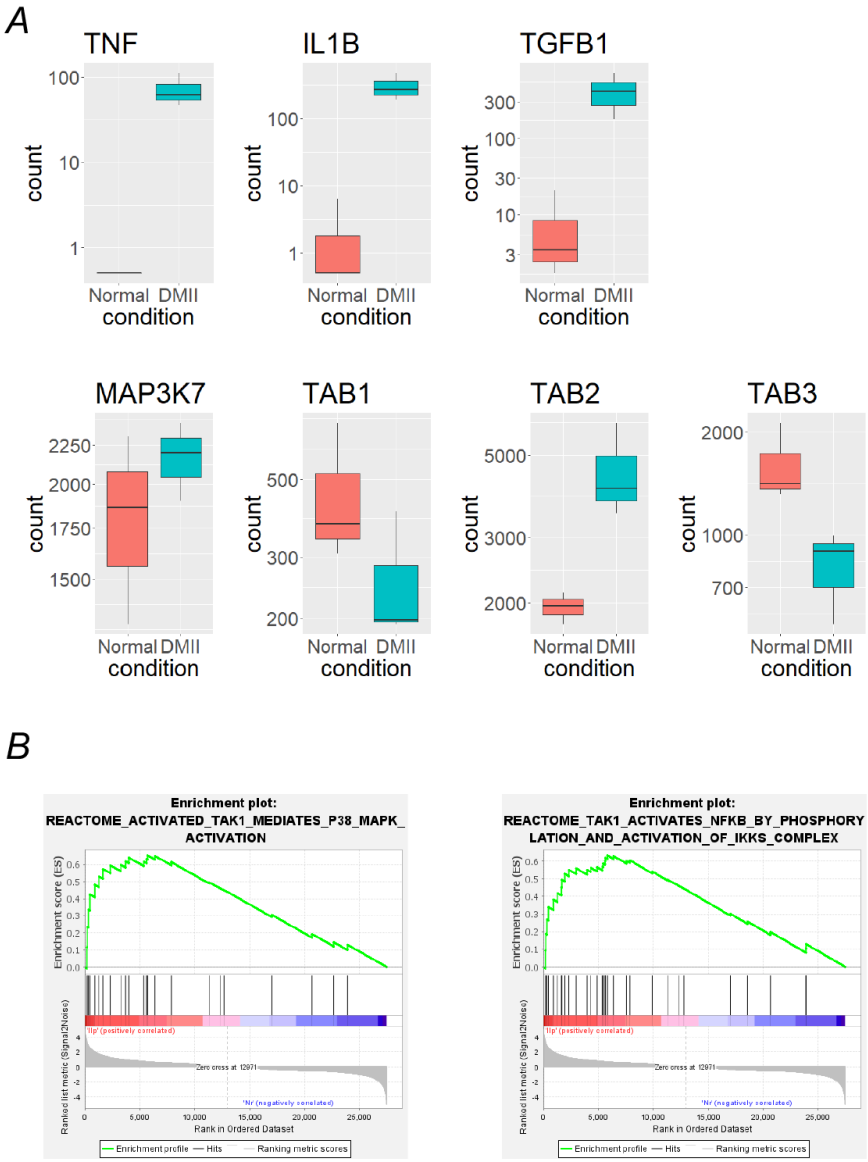

Fig. S3 (A) Readcounts of selected genes related to TAK1 in retinae from normal control and patients with retinal neovascularization due to diabetic retinopathy. (B) Positively enriched gene sets identified by the GSEA in the gene sets collection for canonical pathways. False discovery rate (FDR) was set at a q value <0.05.

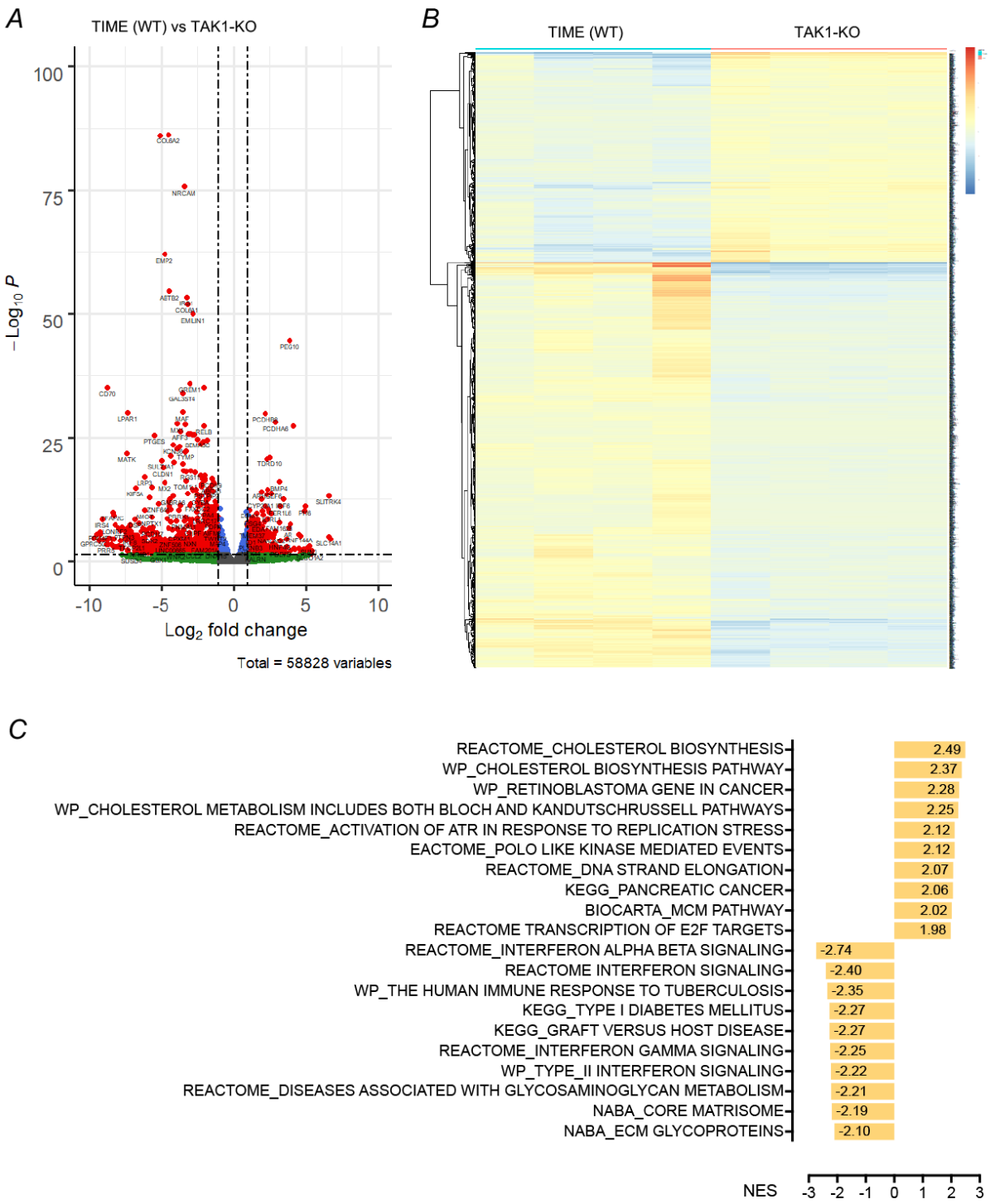

Fig. S4 (A) Volcano plots showing genes were significantly different between wild type and TAK1-KO TIME cells. Red dots refer to genes showing a log2|fold change| > 1 and FDR < 0.05. Labels indicate the significantly up-regulated genes in each data set. (B) Heat map showing all the genes that were different between wild type (WT) and TAK1-KO TIME cells (n=4). (C) GSEA revealed that TAK1-KO led to deficient immune response in TIME cells.

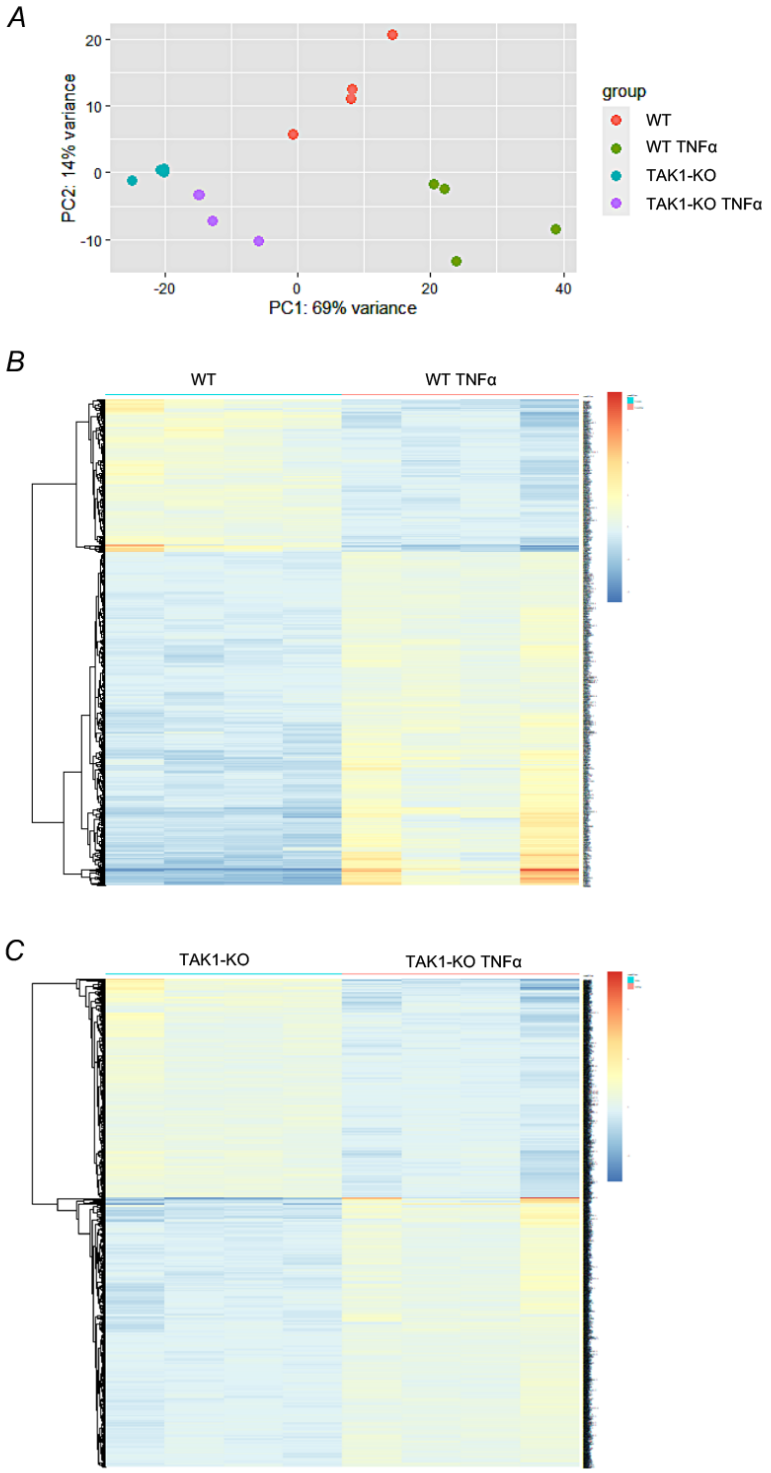

Fig. S5 (A) Principal components analysis of RNA-seq data of wild type cells, wild type cells treated with TNFα, TAK1-KO cells, and TAK1-KO cells treated with TNFα. Each dot represents an experimental replicate. (B) Heat map showing all differentially expressed genes between wild type TIME cells and wild type (WT) TIME cells treated with TNFα. (C) Heat map showed all differentially expressed genes between TAK1-KO TIME cells and TAK1-KO TIME cells treated with TNFα.

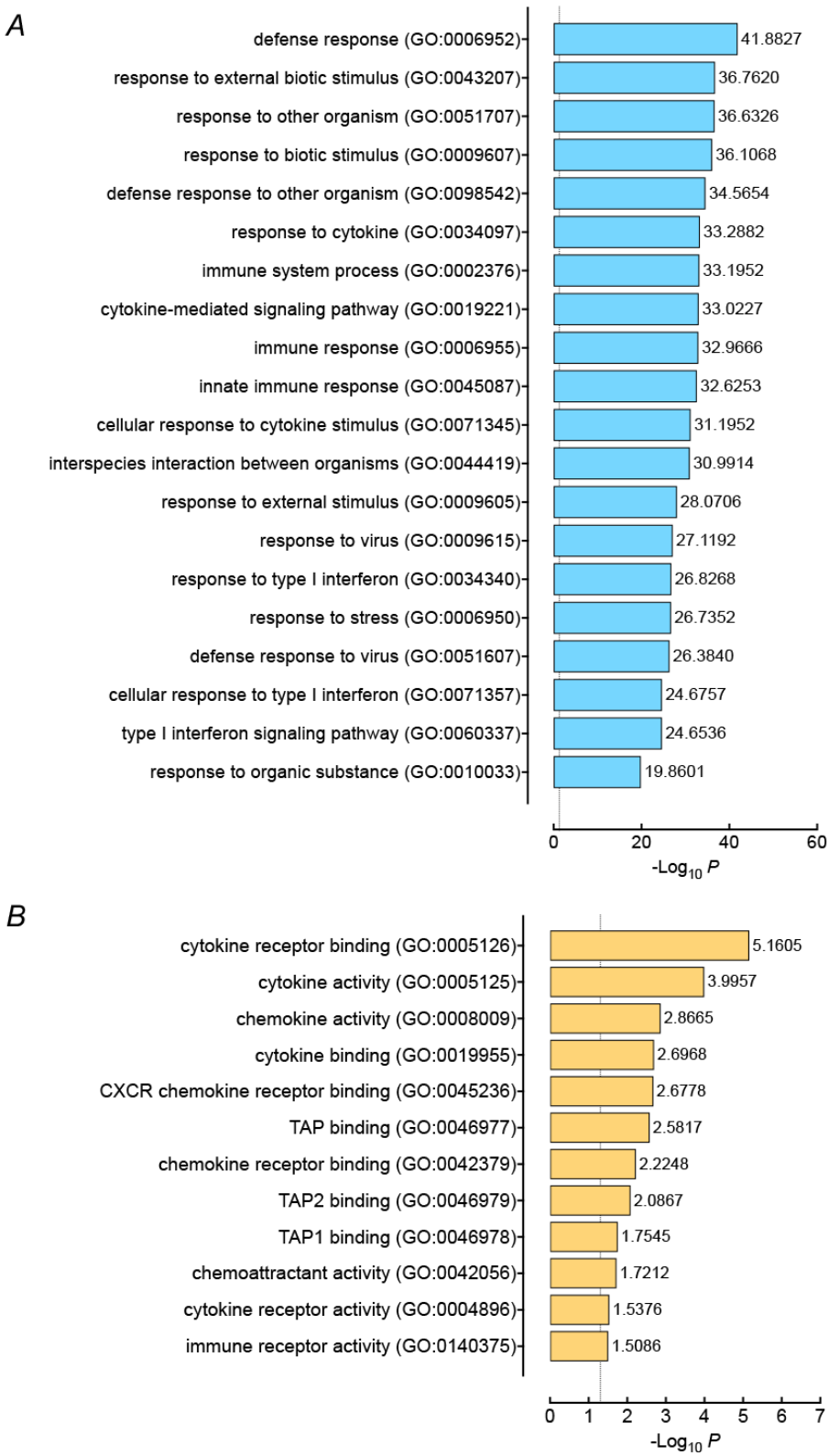

Fig. S6 (A) Gene Ontology revealed biological processes affected by TAK1-KO in TIME cells stimulated by TNFα treatment. (B) Gene Ontology revealed molecular functions affected by TAK1-KO in TIME cells stimulated by TNFα treatment.

Cytokines/chemokines and their modulators

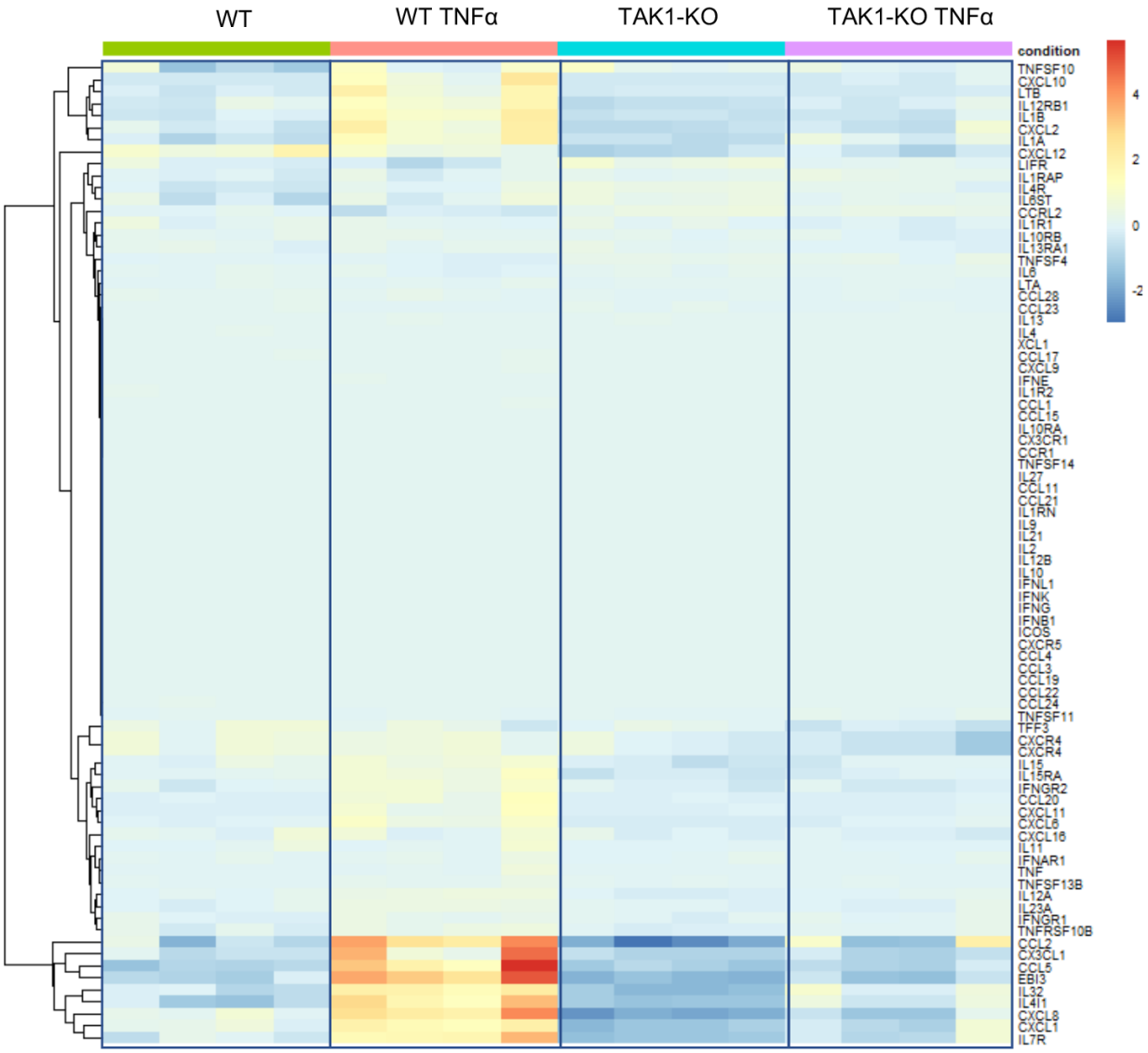

Fig. S7 Heat map generated from unsupervised clustering of cytokines/chemokines genes and their modulators, a function category of NFκB targets (FDR < 0.05).

Growth factors, ligands, and their modulators

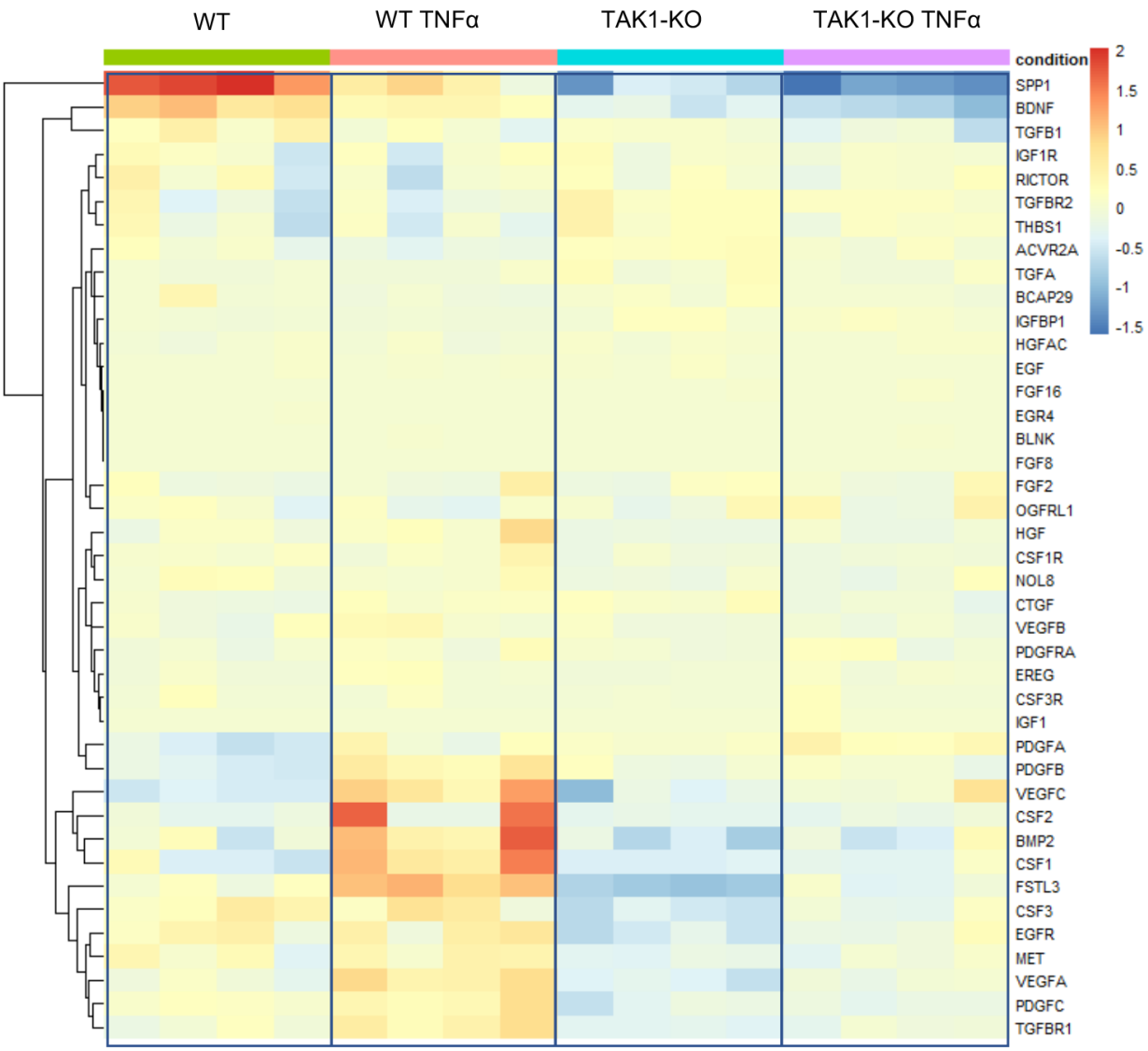

Fig. S8 Heat map generated from unsupervised clustering of genes in the growth factors, ligands, and their modulators, a functional category of NFκB targets (FDR < 0.05).

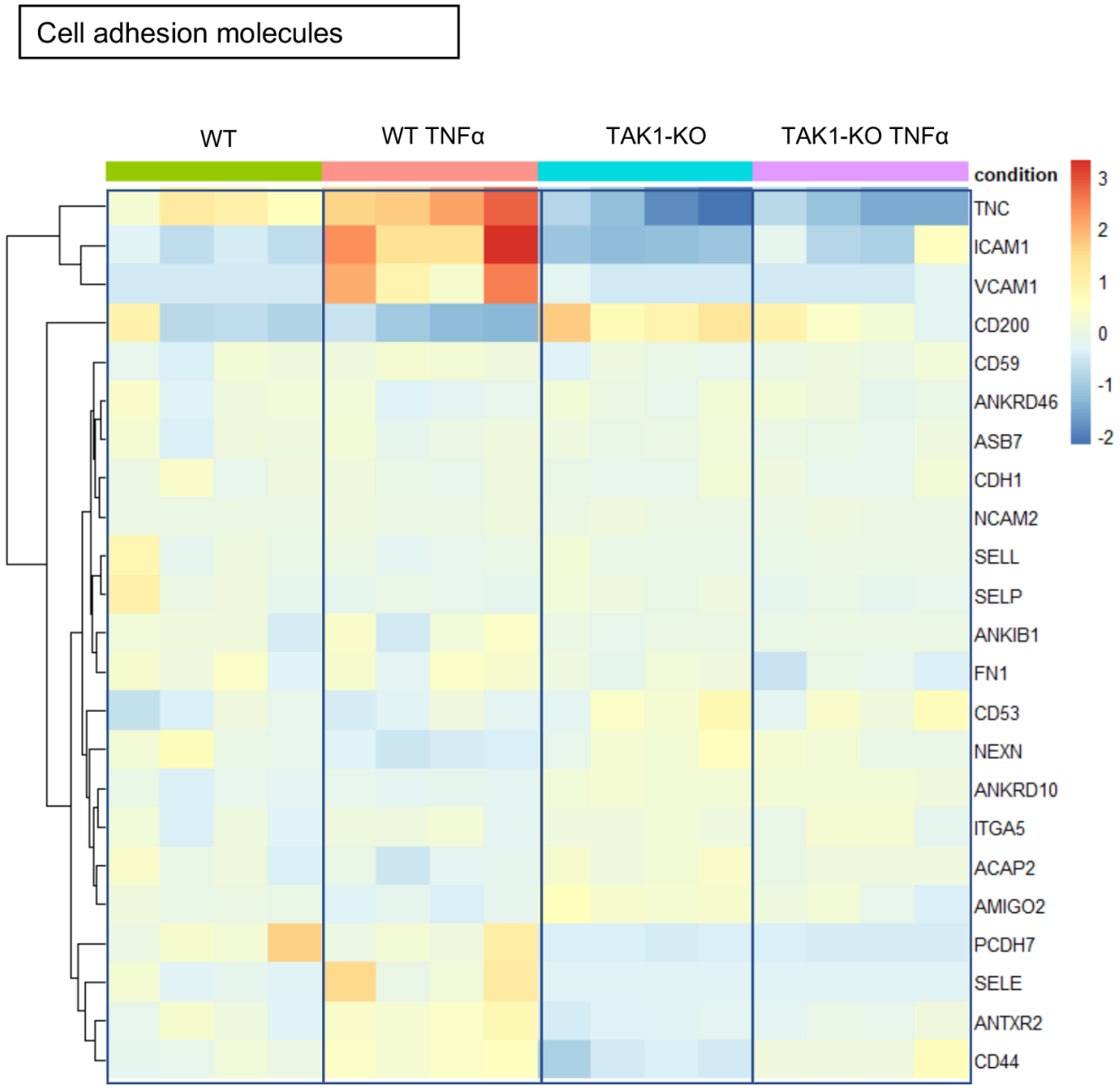

Fig. S9 Heat map generated from unsupervised clustering of genes in the cell adhesion molecules, a functional category of NFκB targets (FDR < 0.05).

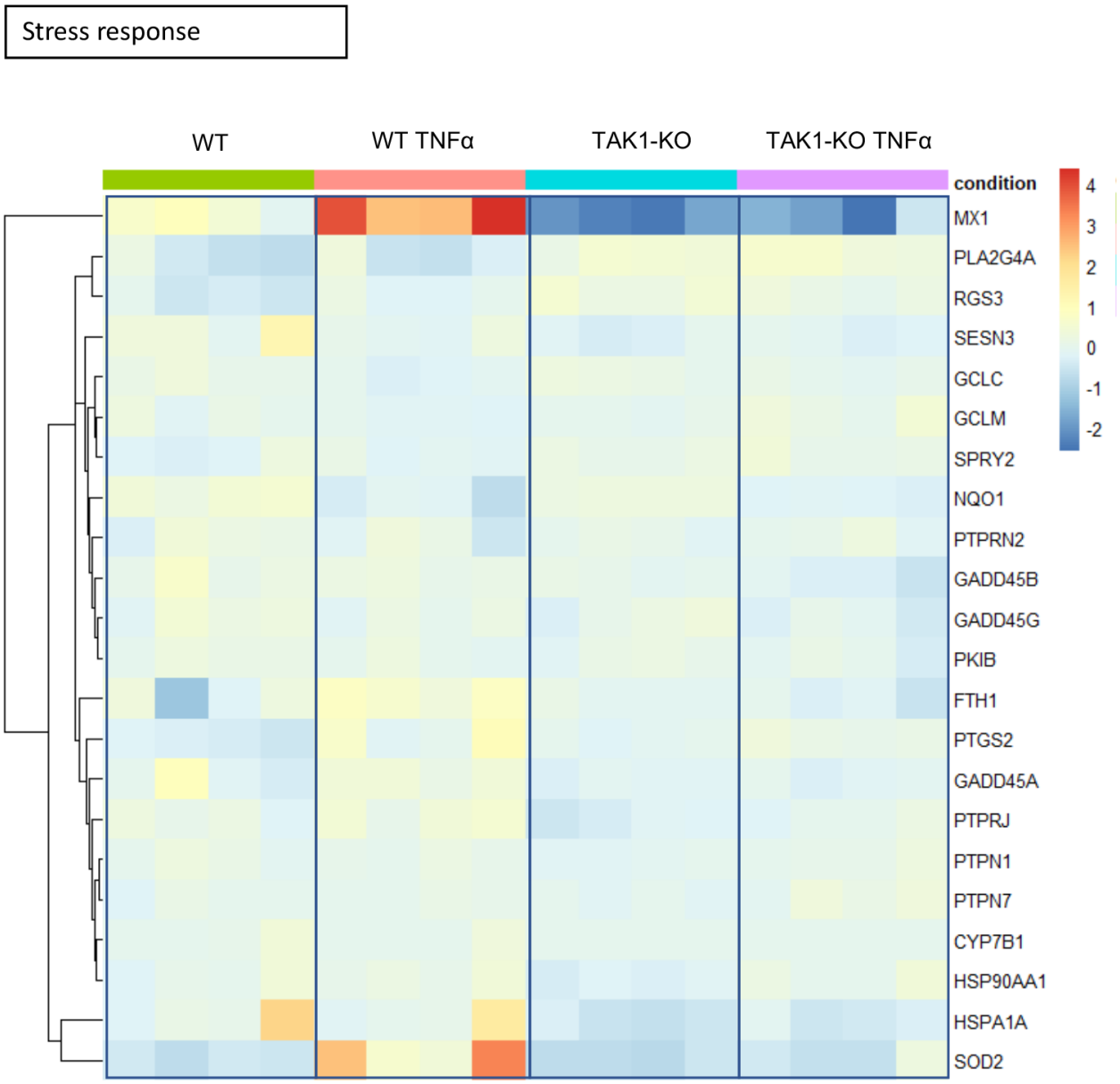

Fig. S10 Heat map generated from unsupervised clustering of genes in the stress response, a functional category of NFκB targets (FDR < 0.05).

Regulators of apoptosis

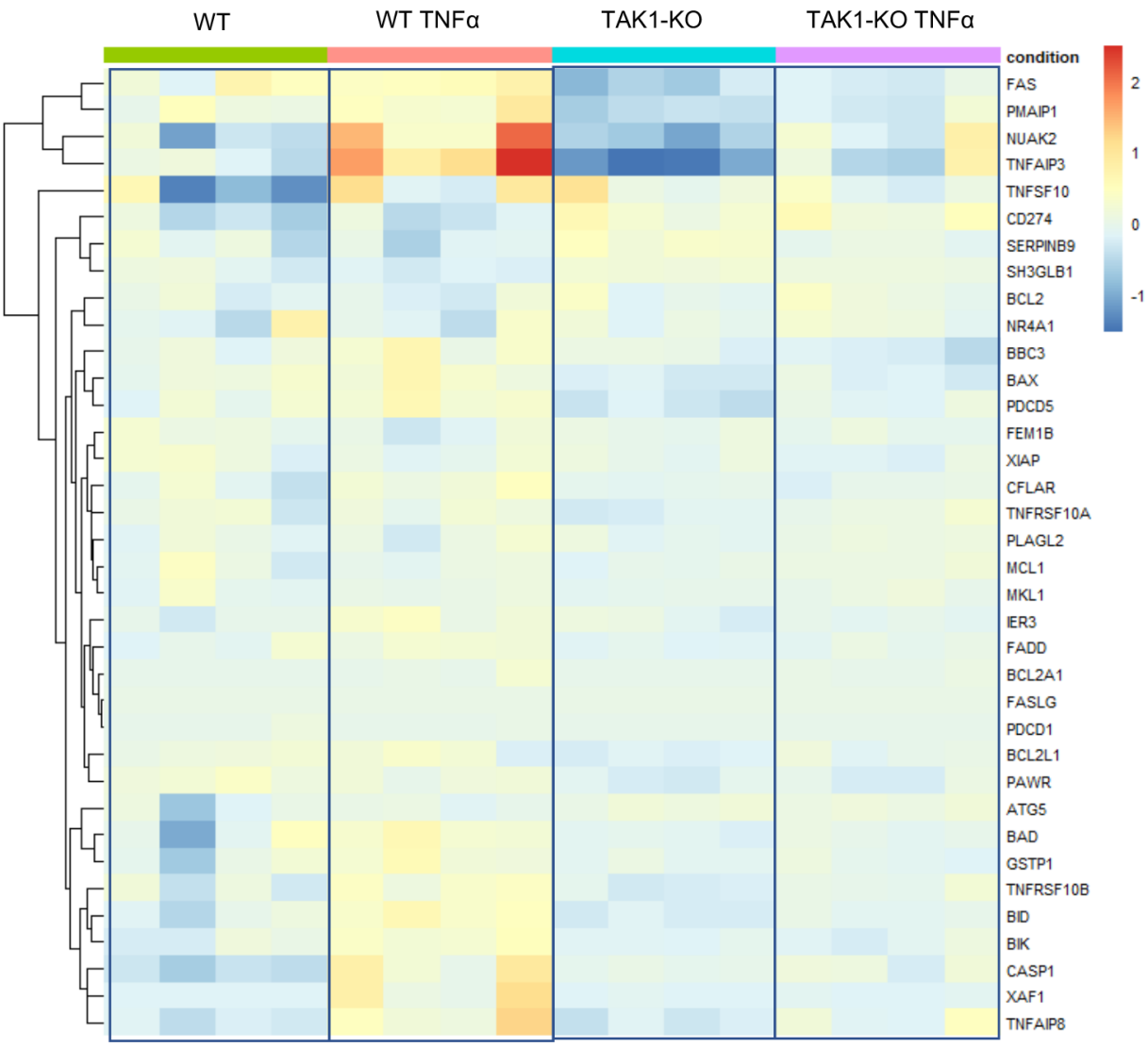

Fig. S11 Heat map generated from unsupervised clustering of genes in the regulators of apoptosis, a functional category of NFκB targets (FDR < 0.05).

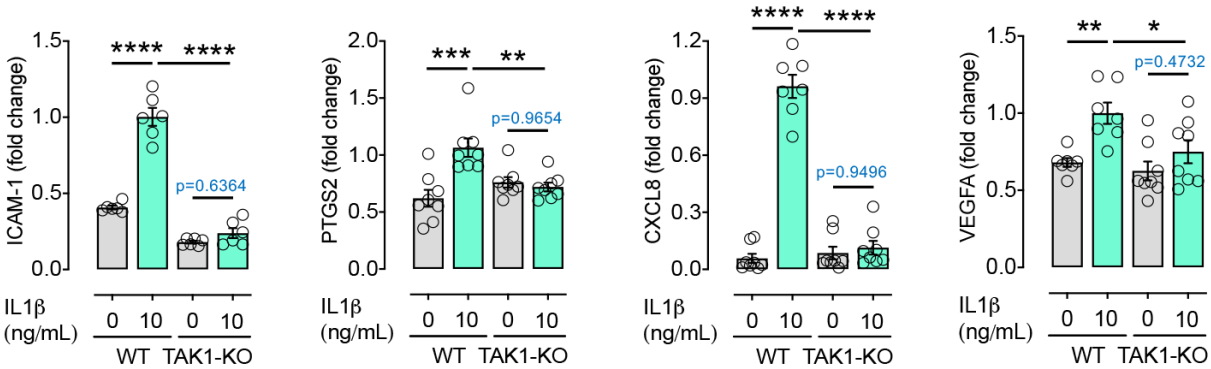

Fig. S12 qPCR results showing that TAK1-KO suppressed *ICAM-1*, *PTGS2* and *CXCL8* but *VEGFA* expression in TIME cells driven by IL1β stimulation for 24 hours (n=4; technical duplicate from each biological repeat was shown as separated dot plot). All data are shown as means ± SEM. Statistical analysis was undertaken with one-way ANOVA and Tukey's multiple comparison test; **P* < 0.05, ***P* < 0.01, ****P* < 0.001, *****P* < 0.0001.

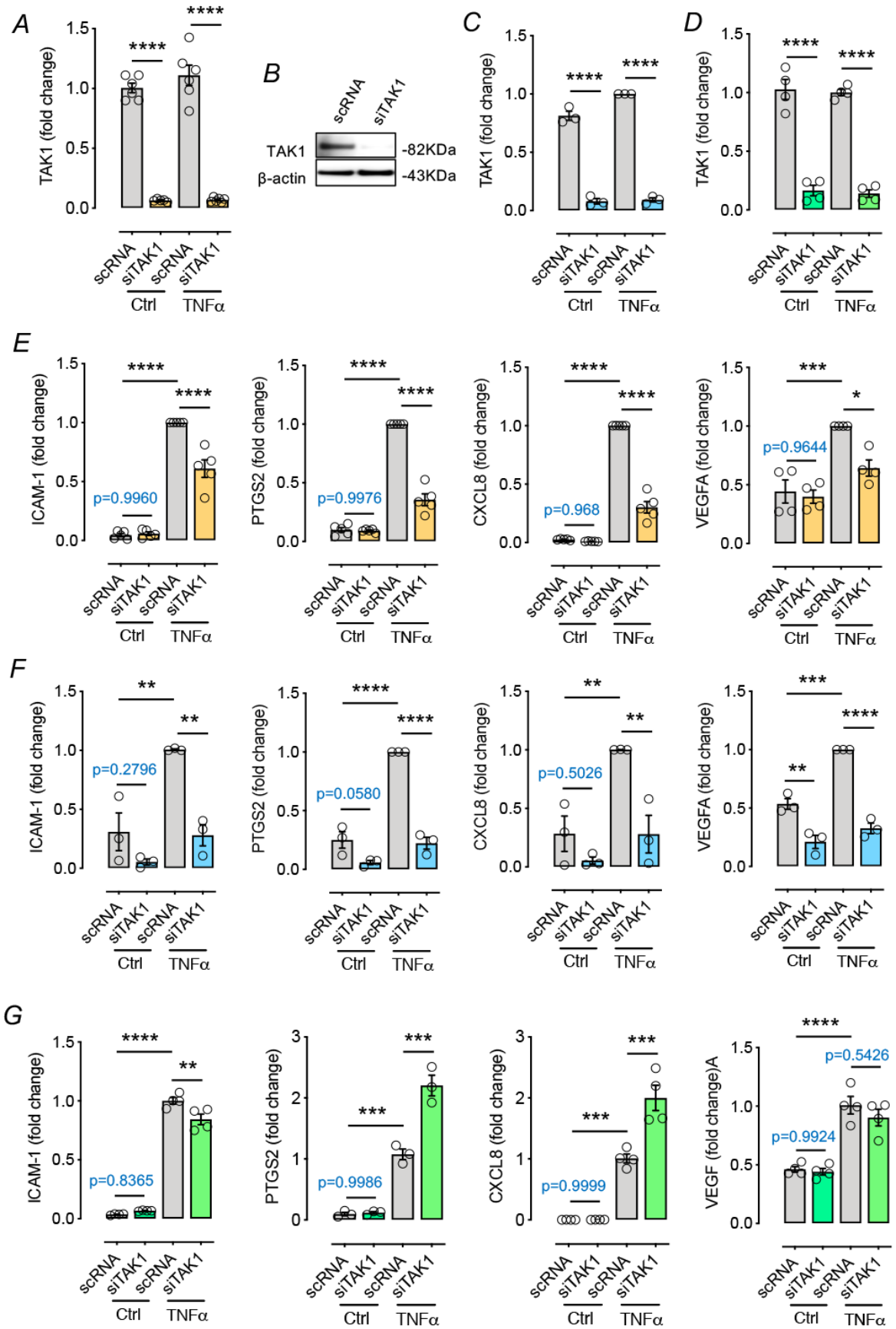
A
TAK1 (fold change)
1.5
1.0
0.5
0.0
****
****
scRNA
siTAK1
scRNA
siTAK1
Ctrl
TNFα
B
scRNA
siTAK1
TAK1
β-actin
-82KDa
-43KDa
C
TAK1 (fold change)
****
****
scRNA
siTAK1
scRNA
siTAK1
Ctrl
TNFα
D
TAK1 (fold change)
****
****
scRNA
siTAK1
scRNA
siTAK1
Ctrl
TNFα
E
ICAM-1 (fold change)
****
****
p=0.9960
scRNA
siTAK1
scRNA
siTAK1
Ctrl
TNFα
PTGS2 (fold change)
****
****
p=0.9976
scRNA
siTAK1
scRNA
siTAK1
Ctrl
TNFα
CXCL8 (fold change)
****
****
p=0.968
scRNA
siTAK1
scRNA
siTAK1
Ctrl
TNFα
VEGFA (fold change)
***
*
p=0.9644
scRNA
siTAK1
scRNA
siTAK1
Ctrl
TNFα
F
ICAM-1 (fold change)
**
**
p=0.2796
scRNA
siTAK1
scRNA
siTAK1
Ctrl
TNFα
PTGS2 (fold change)
****
****
p=0.0580
scRNA
siTAK1
scRNA
siTAK1
Ctrl
TNFα
CXCL8 (fold change)
**
**
p=0.5026
scRNA
siTAK1
scRNA
siTAK1
Ctrl
TNFα
VEGFA (fold change)
***
****
**
scRNA
siTAK1
scRNA
siTAK1
Ctrl
TNFα
G
ICAM-1 (fold change)
****
**
p=0.8365
scRNA
siTAK1
scRNA
siTAK1
Ctrl
TNFα
PTGS2 (fold change)
***
***
p=0.9986
scRNA
siTAK1
scRNA
siTAK1
Ctrl
TNFα
CXCL8 (fold change)
***
***
p=0.9999
scRNA
siTAK1
scRNA
siTAK1
Ctrl
TNFα
VEGF (fold change)A
****
p=0.5426
p=0.9924
scRNA
siTAK1
scRNA
siTAK1
Ctrl
TNFα

1058

1059 **Fig. S13** *TAK1* knockdown by siRNA reduced the expression of proinflammatory and pro-angiogenic
1060 genes in human endothelial cells but not human Muller cells. (A) *TAK1* expression was compared in
1061 wild type, TAK1 knockdown by siRNA targeting TAK1 (siTAK1) TIME cells and those cells treated
1062 with TNFα, using qPCR (each dot represents a biological repeat). (B) Western blot analysis of TAK1
1063 knockdown by siTAK1 in TIMEs. (C-D) Under the same treatment conditions as Fig. S13A, *TAK1*
1064 expression was compared in HRMEC and Müller cells using qPCR. (E-G) Expression of *ICAM-1,*
1065 *PTGS2, CXCL8 and VEGF* was compared in TIMEs, HRMECs and Müller cells. All data are shown
1066 as means ± SEM. Statistical analysis was undertaken with one-way ANOVA and Tukey's multiple
1067 comparison test; *$P < 0.05$, **$P < 0.01$, ***$P < 0.001$, ****$P < 0.0001$.
1068
1069

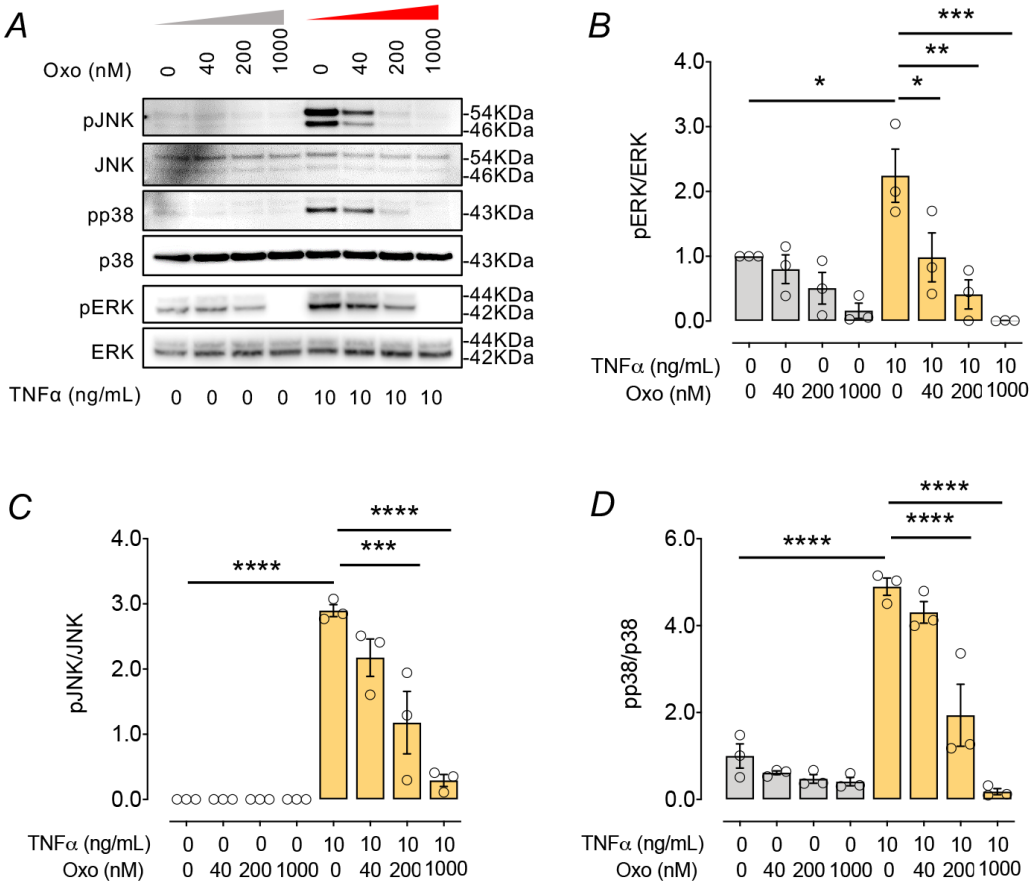

Fig. S14 Pharmacological inhibition of TAK1 by 5Z-7-oxozeaenol (Oxo) suppressed MAPK pathways in TIMEs. (A) TIME cells were pretreated with 5Z-7-oxozeaenol (Oxo) (40, 200 or 1000 nM) for 30 minutes, followed by TNFα stimulation (10 ng/ml) for 10 minutes. Activation of ERK, JNK, and p38 was assessed by western blot (n = 3). (B-D) Western blot showed that pharmacological inhibition of MAPK (ERK, JNK and p38) activation in TIMEs. All data are shown as means ± SEM. Statistical analysis was undertaken with one-way ANOVA and Tukey's multiple comparison test; *$P < 0.05$, **$P < 0.01$, ***$P < 0.001$, ****$P < 0.0001$.

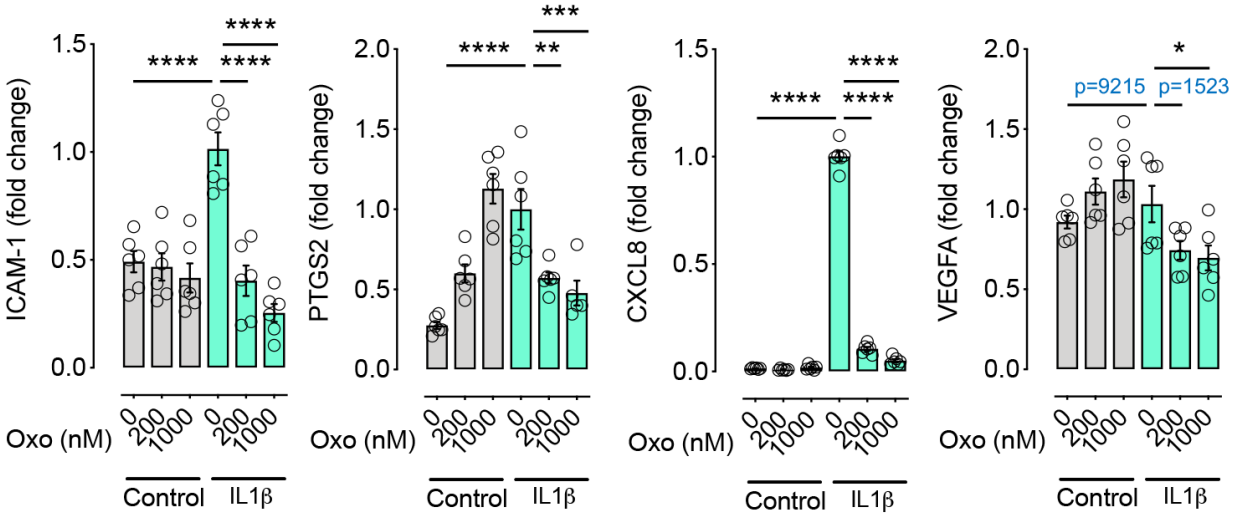

Fig. S15 qPCR results revealed that Pharmacological inhibition of TAK1 by 5Z-7-oxozeaenol (Oxo) suppressed *ICAM-1*, *PTGS2*, *CXCL8* and *VEGFA* in HRMECs stimulated with IL1β in a dose-dependent manner. All data are shown as means ± SEM. Statistical analysis was undertaken with one-way ANOVA and Tukey's multiple comparison test; **P* < 0.05, ***P* < 0.01, ****P* < 0.001, *****P* < 0.0001.

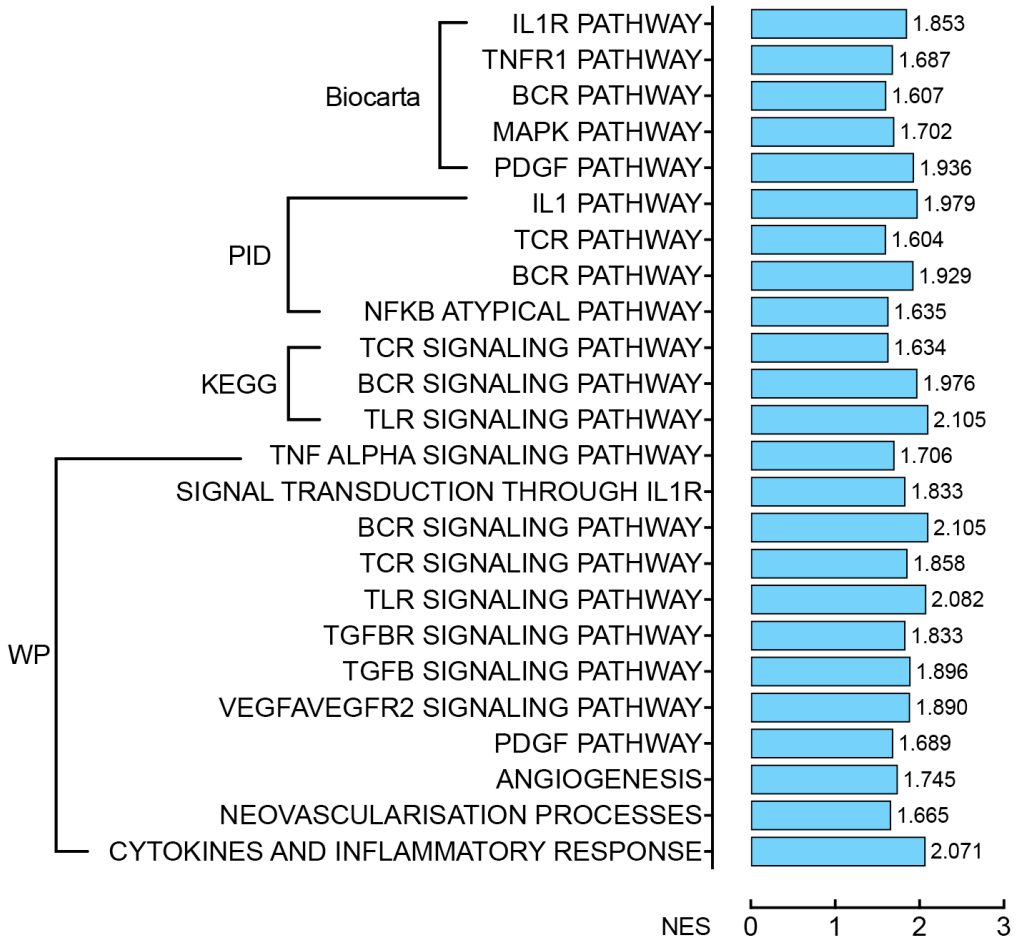

Fig. S16 Gene-set enrichment analysis from multiple databases indicated the positive impact of TAK1 upstream pathways in rat OIR retinas. Genome-wide transcriptional analysis of rat OIR retina samples indicated the differential gene expression associated with positive impact in TAK1 upstream pathways. Biocarta, Pathway Interaction Database (PID), Kyoto Encyclopedia of Genes and Genomes (KEGG), and WikiPathways (WP) gene sets were used in GSEA.

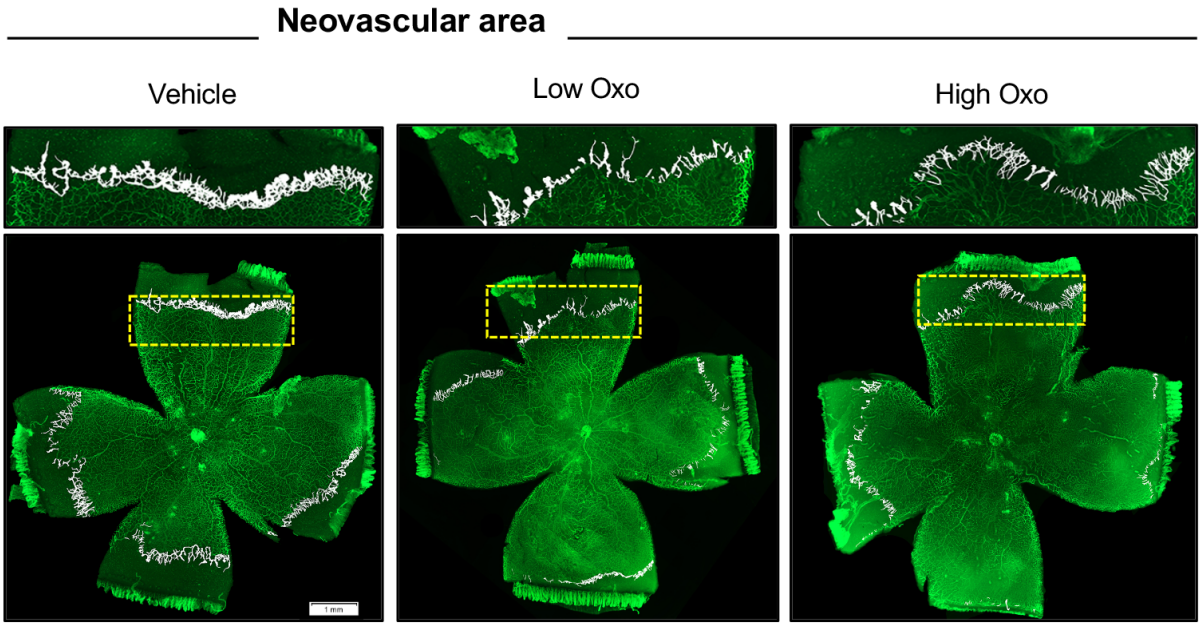

Fig. S17 Uncropped retinal flat mounts. The region indicated by the dashed line was used to show retinal neovascularization (highlighted in white) in Fig. 7C. Oxo: 5Z-7-oxozeaenol. Scale bar: 1 mm.

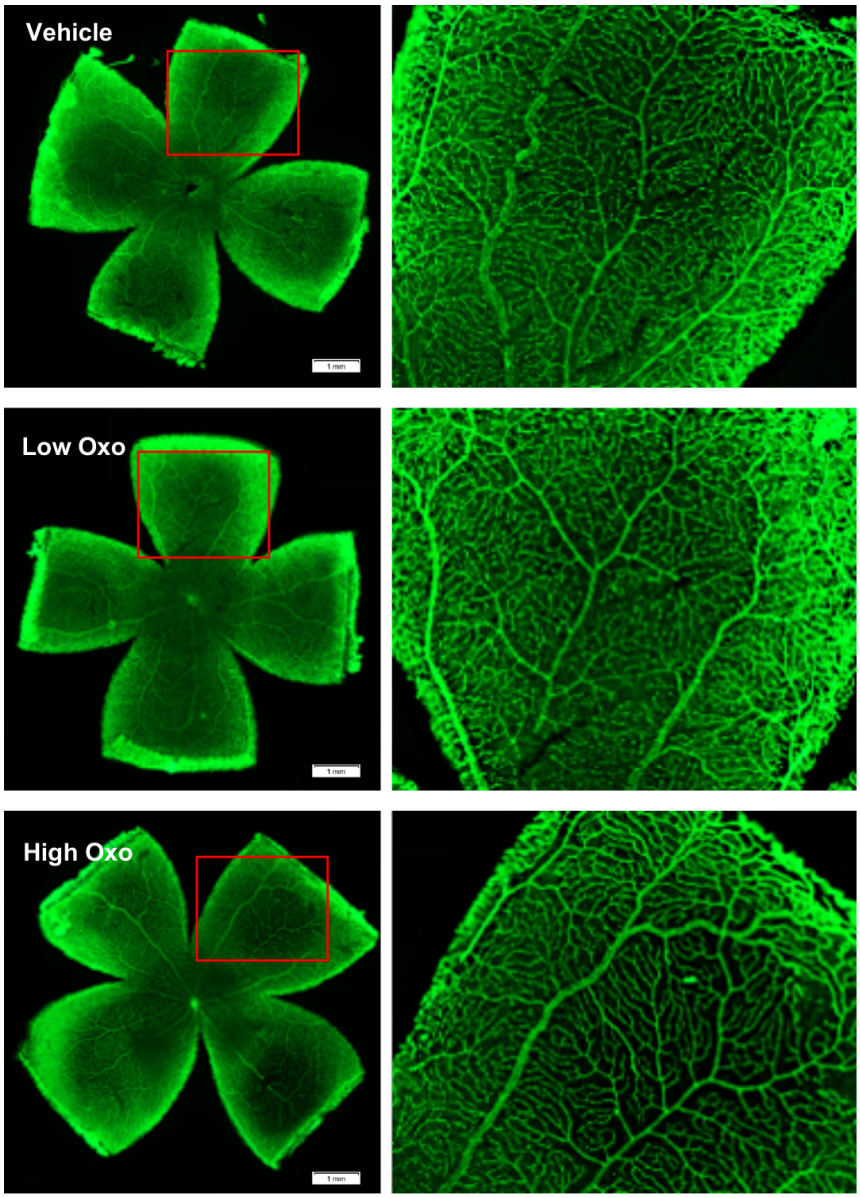

Fig. S18 Inhibition of TAK1 did not cause retinal vessel remodeling. Retinal flat mount was labelled with IB4 28 days after a single intravitreal injection of vehicle, low (18 ng) or high (90 ng) dose of 5Z-7-oxozeaenol (Oxo) in normoxic rats to examine drug effects on normal retinal vasculature. Scale bar: 1 mm.

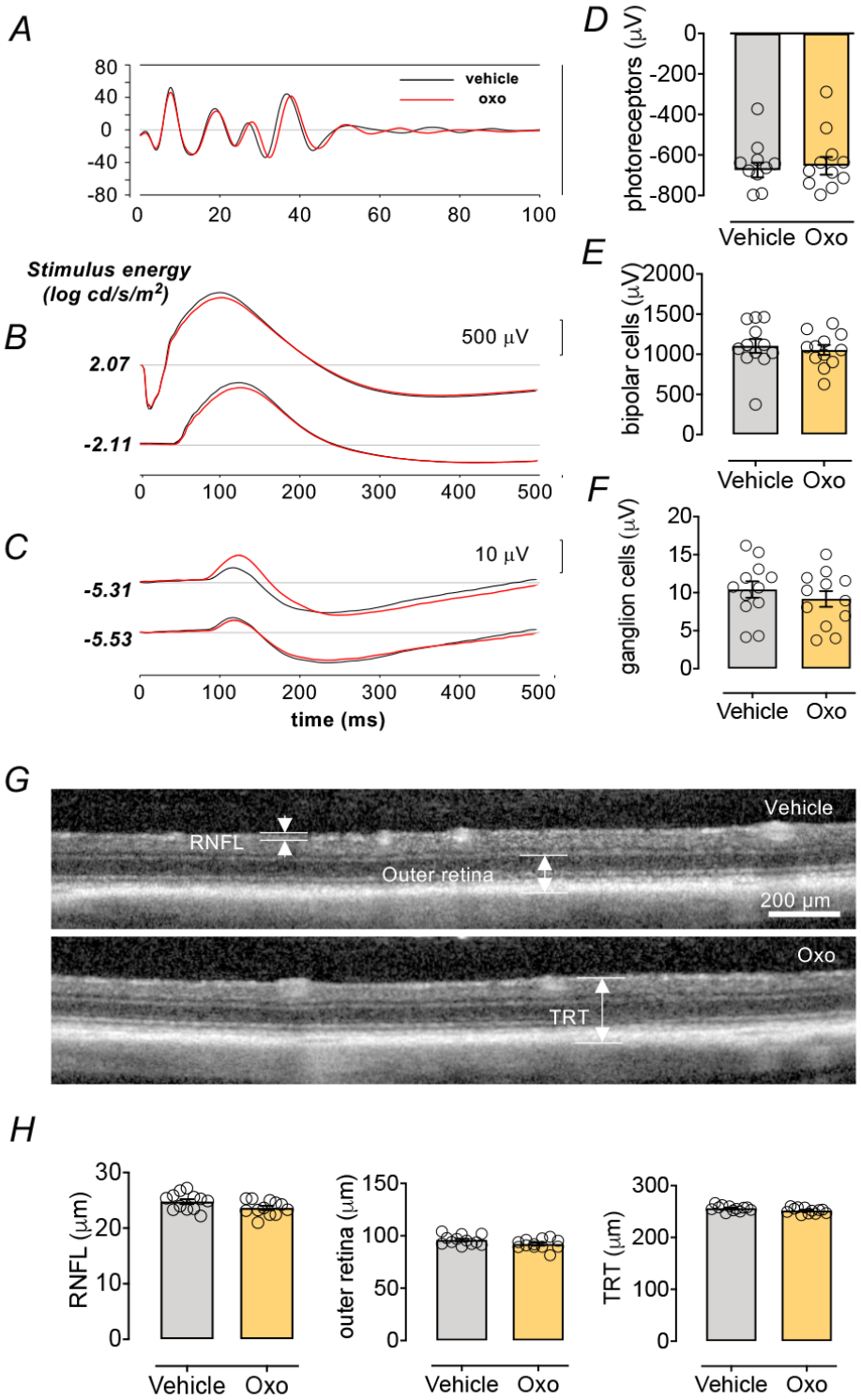

Fig. S19 Effect of 5Z-7-oxozeaenol (Oxo) on *in vivo* retinal structure and function. ERG and OCT were performed 28 days after intravitreal injection of 5Z-7-oxozeaenol (90 ng) in normoxia Brown Norway rats. No difference was observed between the vehicle- (black traces) and 5Z-7-oxozeaenol-injected (red traces) eyes in terms of the average amacrine cell oscillatory potentials (A) photoreceptoral and bipolar cell responses (B) or ganglion cell responses (C) in 5Z-7-oxozeaenol-

1114 injected eyes (n=11, red traces) and corresponding vehicle-injected eyes (n=12, black traces). Group
1115 average (± SEM) photoreceptor (D. *P*=0.71) bipolar cell (E. *P* = 0.63) and ganglion cell (F, *P*=0.41).
1116 Response amplitude were not different between 5Z-7-oxozeaenol-injected eyes and corresponding
1117 vehicle-injected eyes. (G) Representative OCT images from a 5Z-7-oxozeaenol- and vehicle-injected
1118 eye. (H) Total retinal thickness (TRT), outer retina, and retinal nerve fiber layer (RNFL) thickness
1119 were not different between groups (*P*=0.0639 of TRT, *P*=0.0502 of outer retina, *P*=0.064 of RNFL).
1120 All data are shown expressed as means ± SEM. Statistical analysis was undertaken with two-tailed
1121 Student's *t*-test.